Chapter 7
In-vitro Cell Line studies

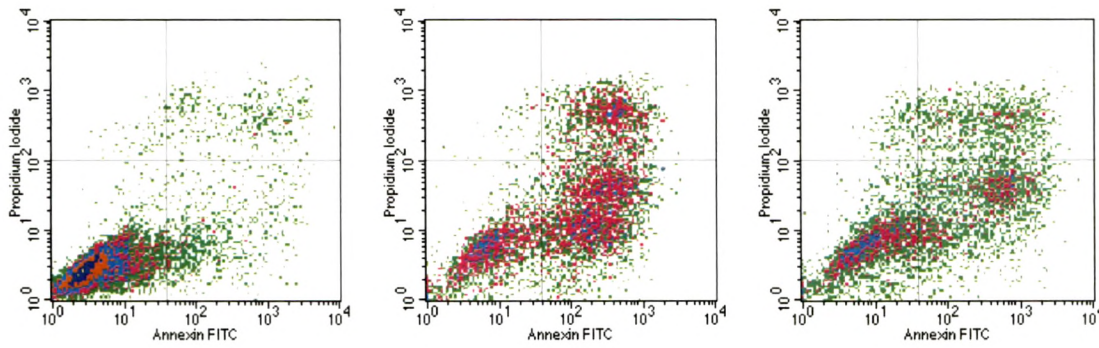

7.1. Introduction

Breast cancer accounts for more deaths of United States women than any other type of malignancy (National cancer Institute 2009). Breast cancer incidence in women in the United States is 1 in 8 (about 13%). There are more than 50 types of different breast cancer cell lines. The criteria considered for the selection of cell lines were Population doubling time (PDT) and expression of receptors for targeting moiety. The MDA-MB-231 and BT-20 cell lines were chosen for the *in vitro* cell culture experiments. The MDA-MB-231 and BT-20 are cell lines of human origin from mammary gland tissue. It was cultured as a monolayer. It is an adherent cell line.

Cell cycle

In order for a living organism to grow their individual cells must increase in size, make exact replicas of all their genetic material, and then go through a process of division. This results in two daughter cells each with one complete copy of the genome. The *eukaryotic cell* of a higher organisms, ranging from yeast to humans, has its genetic material (DNA) is packaged into a membrane bound nucleus. In eukaryotic cells the process of cell growth and division, the cell cycle, is characterized by four distinct phases.

Quiescence: Cells which are not proliferating are said to be quiescent or in "G0" phase.

G1 Phase: During the first phase (G1) cells grow in size in response to mitogenic signals, such as soluble extracellular growth factors and intracellular contact, which may trigger a commitment to entering the next phase of the cell cycle.

The Restriction Point: Late in G1, many cell types become committed to entering the next phase of the cell cycle at a time termed the *restriction point*. The existence of a restriction point can be demonstrated by the simple act by depriving cells from growth factors in their medium. Many types of cells will continue to complete a single cell cycle, if they are in S-phase, G2 or Mitosis, but will then arrest in the next G1 phase.

S-Phase: Soon after the restriction point a cell begins to replicate its genetic material through the activity of a family of enzymes including the DNA polymerases, which are capable of synthesizing an exact replica of the DNA genome. In a mere 6-hours the cell polymerizes exact replicas of all 46 chromosomes, totaling six billion nucleotides, while

maintaining the identical sequence of nucleotides as the parental DNA and thus preserving the genetic information. This *"S-phase"* of the cell cycle is thus biochemically distinct from the other phases of the cell cycle and can easily be distinguished from other cells by their ability to stably incorporate fluorescently or radioactively tagged nucleotides, the building blocks of DNA, into their chromosomes.

G2 Phase: At the completion of S-phase, DNA replication ceases and cells enter the G2 phase of the cell cycle.

Mitosis: *Mitosis* is the phase of the cell cycle in which cells physically divide into two separate daughter cells. In order to do so they first dissolve the nuclear membrane which will later reform once cell division is complete. The DNA-containing chromosomes then condense into structures so compact that they can be seen with a light microscope. The chromosomes then precisely segregate to two sides of the cell, such that each half of the cell gets exactly one copy of each chromosome. At the completion of mitosis, cells undergo *cytokinesis* or separation into two halves. This occurs as a band forms around the circumference outer plasma membrane which gradual constricts like a belt until the cell pinches in two and the two daughter cells once again enter G1.

Cell cycle analysis based on measurements of DNA content generates a clear pattern of distribution: G0/G1 phase (one set of paired chromosomes per cell), S phase (DNA synthesis with variable amount of DNA), and G2/M phase (two sets of paired chromosomes per cell, prior to cell division) (Shapiro, H.M. et al., 2003) DNA content can be measured using fluorescent, DNA-selective stains that exhibit emission signals proportional to DNA mass. Flow cytometric analysis of these stained populations is then used to produce a frequency histogram that reveals the various phases of the cell cycle. This analysis is typically performed on permeabilized or fixed cells using a cell-impermeant nucleic acid stain, but is also possible using live cells and a cell-permeant nucleic acid stain. While the choices for fixed-cell staining are varied, there are only a few examples of useful cell-permeant nucleic acid stains.

Nuclear DNA is one of the parameters measured by flow cytometry. This measurement calculates the percentage of a cell population in each phase of the classic cell cycle. The

percentage of cells in the S-phase gives an indication of the proliferative activity of that cell population.

The flow cytometer can indicate relative cell size and density or complexity by measuring forward- and side-scattered laser light, respectively. In addition, the flow cytometer can measure relative fluorescence from fluorescent probes which bind to specific cell-associated molecules. These fluorescent probes are often fluorochrome-labeled antibodies specific for cell surface molecules, but may also be nucleic acid probes (e.g. Propidium Iodide), cell function probes (e.g. Indo-1), or fluorescent proteins (e.g. GFP). As the labeled cells flow past a laser beam, the probes fluoresce, and the emitted light is directed to detectors which translate the light signals into information concerning the relative fluorescent intensity associated with each cell.

Flow cytometry measures the percentage of cells in a population with each (or multiple) fluorescent probe(s) attached. The cell sorter is capable of sorting specific cell populations from a mixture of cells based on fluorescence profiles.

The most commonly used dye for DNA content/cell cycle analysis is propidium iodide (PI). It can be used to stain whole cells or isolated nuclei. The PI intercalates into the major groove of double-stranded DNA and produces a highly fluorescent adduct that can be excited at 488 nm with a broad emission centered around 600 nm. Since PI can also bind to double-stranded RNA, it is necessary to treat the cells with RNase for optimal DNA resolution.

Apoptosis

Animal cells can self-destruct via an intrinsic program of cell death (Steller et al., 1995). Apoptosis is a form of programmed cell death that is characterized by specific morphologic and biochemical properties (Wyllie et al., 1980). Morphologically, apoptosis is characterized by a series of structural changes in dying cells: blebbing of the plasma membrane, condensation of the cytoplasm and nucleus, and cellular fragmentation into membrane apoptotic bodies (Steller et al., 1995; Wyllie et al., 1980).

Apoptosis is a complex phenomenon of related morphological and biochemical processes that can vary with tissue and cell type (Zakeri et al., 1995). The protein Bcl-2 appears localized or associated with intracellular membranes of mitochondria, endoplasmic reticulum, and nuclei (Reed et al., 1994). Although the mechanism of Bcl-2 action is

unknown, biochemical studies have implicated this protein in the regulation of the redox potential of the cell, as ecotopic expression of bcl-2 suppresses cell death induced by oxidizing agents and appears to affect glutathione levels (Korsmeyer et al., 1993; & Zhong et al., 1993).

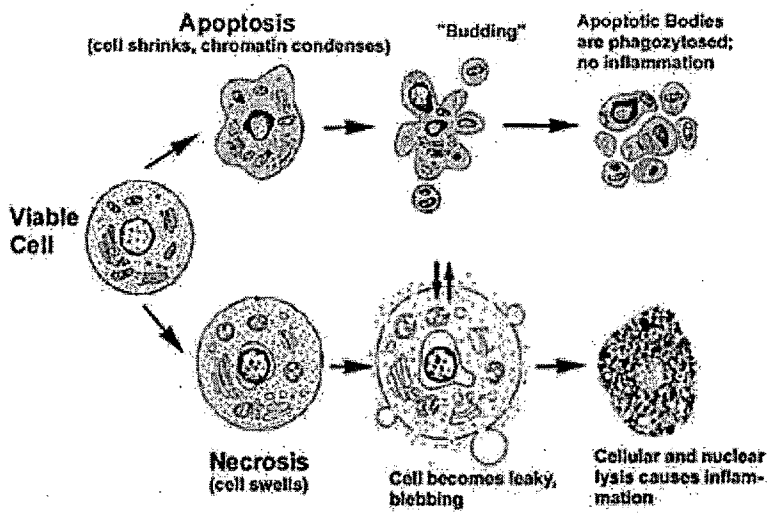

Figure: 7.1. Hallmarks of the apoptotic and necrotic cell death process. Apoptosis includes cellular shrinking, chromatin condensation and margination at the nuclear periphery with the eventual formation of membrane-bound apoptotic bodies that contain organelles, cytosol and nuclear fragments and are phagocytosed without triggering inflammatory processes. The necrotic cell swells, becomes leaky and finally is disrupted and releases its contents into the surrounding tissue resulting in inflammation. Modified from (Cruchten, V. et al., 2002).

Agents like anticancer drugs and ionizing radiation that damage DNA induce apoptosis through a p53-dependent pathway. Binding of p53 and other nuclear proteins to the sites of damage in the DNA appears to trigger the apoptotic process. Another mechanism that can induce apoptosis involves the interaction of proteins such as Fas (CD95) or tumor necrosis factor with their receptors on the surface of cells. Signaling from these so-called death receptors starts the apoptotic process. The characteristic of cells undergoing apoptosis is the capacity to bind the protein Annexin V (AV). AV binds to Phophotydile Serin (PS), which is normally located on the inner leaflet of the plasma membrane, but it is externalized to the outer leaflet during apoptosis. PI staining is widely used to discriminate living cells, which exclude this DNA dye, from dead cells, which are permeable to it. In populations of cells undergoing apoptosis, there are some cells that bind AV but are not stained with PI. This "single-positive" population is thought to

represent cells in an early stage of apoptosis because the cells apparently exclude PI and because it appears earlier than DNA ladders can be seen (Eliason, J.F. et al., 2000).

Table: 7.1. Materials and equipments

Material	Source
Water (Double distilled)	Prepared in laboratory by distillation
BT-20 and MDA-MB-231 cells	ATCC
Dulbecco's Modified Eagle Medium (DMEM), HAM's F-10 medium, , fetal bovine serum and streptomycin-penicillin, Phosphate buffer saline	ATCC
6-Coumarin	Gift sample from Neelikon dyes, Mumbai, India
Dimethyl Sulfoxide, Triton X-100	ATCC
Sodium hydroxide	S.D.Fine chemicals, Mumbai, India
CCK-8 reagent	DOJindo Molecular Tech. Inc., Maryland
Nuclepore Polycarbonate membrane0.2, 0.45 and 2 μm 25mm	Milipore, Whatman, USA.
Equipments	**Source/Make**
Calibrated pipettes of 1.0 ml, 5.0 ml and 10.0 ml, volumetric flasks of 10 ml, 25 ml, 50 ml and 100 ml capacity, Funnels (i.d. 5.0 cm), beakers (250 ml) and other requisite glasswares,	Tarsons Ltd., Mumbai
Tissue culture flasks (T 75, T25), 96-well plates, 24-well plates, 35mm PD serological pipettes 1.0 ml, 5.0 ml and 10.0 ml,	Tarsons, Ltd
Micropipette	Brand, Germany
Analytical balance	Precisa 205A SCS, Switzerland
pH meter	Labindia, India
Media Bottles 250ml, 500ml, 1000ml	Durga glasswares Ltd, Baroda
Microtitre plate reader	Synergy HT & Powerwave XS, Biotek, Vermont, USA
Fluoroscent Microscope	Olympus BX61, Japan

7.2. Methods

7.2.1. Intracellular uptake studies

To study the influence of time and concentration on the cellular uptake of Nanoconstructs, following experiments were performed. The cellular uptake studies were carried out using the method reported by *Hu et al 2007*. Briefly, the cells were seeded at a density of 5 X 10^3 cells/well in the 96-well plate (black). At 24hrs, the medium in the

plate was changed and plates were kept in the same condition until 80% confluence was reached. The different concentrations (2, 10, 50,100, 200, 500 and 1000μg/ml) of 6-coumarin loaded Nanoconstructs were prepared in culture medium.

To study the influence of the concentration the medium was then replaced with a 100-μl suspension of 6-coumarin loaded nanoparticles of different concentrations. To study the influence of time, the medium was replaced with 100 μl suspensions of 6-coumarin loaded nanoparticles of 100μg/ml & 100 μl of fresh medium and incubated for 0.25, 0.5, 1, 2, 4, 6hrs. For each type of nanoparticles and concentration, a control was kept by adding the corresponding particle concentration in the well. The fluorescence of this well was treated at control i.e. 100%

At the defined time intervals, suspension from the wells was removed and the wells were washed thrice using PBS (pH 7.4). After lysing the cells with 100μl of 0.5% Triton X-100 in NaOH, 100 μl DMSO was added to the wells and the plates were shaken. The plates were read using a microplate reader. The excitation and emission wavelength was 430 and 485 nm, respectively, for 6-coumarin. As 6-coumarin was assumed to be dispersed evenly in the particles, the fluorescence observed was assumed to be linearly proportional to the amount of particles in the cell lysates. The cellular uptake efficiency was given by the ratio between the amount of particles taken up in cells and the amount of those in control and calculated by the following equation

$$\text{Cellular uptake efficiency} = \frac{\text{fluorescence of sample}}{\text{fluorescence of control}} \times 100 \qquad \text{----Equation [7.1]}$$

The results for influence of the incubation time and concentration are shown in Table: 7.3 and Table: 7.2, respectively and in Figure: 7.2 and Figure: 7.1, respectively.

7.2.2. In-vitro Cytotoxicity Studies

The cytotoxicity assay was conducted using CCK-8 assay. The cell viability was determined by a microplate reader. BT-20 and MDA-MB-231 cells were seeded in 96-well plates in Dulbecco's Modified Eagle Medium (DMEM), supplemented with 10% fetal bovine serum, at a density of 5,000 cells/well and allowed to attach overnight. After 24hr, 2X sequential dilutions of each compounds were prepared (DC,PLGA,PLGA-DC,RGD,LP-DC,LP-DC-RGD) in growth medium(GM), blank LP and PLGA in growth medium by using a new 96 well plate at volume of 120 μl/well. The old media from cells was aspirated and fresh 100 μl of GM to cells was added. The diluted compounds

prepared from new plate were transferred to old plate in the volume of 100 µl into wells with adhered cells by starting from the lowest concentration. The plate was incubated for one, two and three population doubling time for both types of cells at 37°C in CO_2 incubator. The working dilution of CCK-8 reagent was prepared. For one plate (10x6well), 700 µl CCK-8 was added to 2800 µl GM. The old media from cells was aspirated and washed with PBS 7.4. 100 µl fresh GM was added to the cell and blank wells before adding CCK-8 reagent. Plates were incubated for 1.5~2 hrs at 37°C after adding 50 µl diluted CCK-8 reagent. The plates were observed using microplate reader (Biotek® Powerwave XS, Vermont, USA) at 450nm with blank well correction. All experiments were performed in triplicate. The absorbance of untreated cells was considered as 100% cell viability and with respect to that, the treated cell viability was calculated.

7.2.3. DNA content anlaysis by flow cytometry

The cell suspension of 0.15 x 10^6 cells/ml was prepared for BT-20 cells in growth medium (GM) and was added 2.0 ml/well in 6 well plates. After 24hr, 2X sequential dilutions of each compounds were prepared (DC,PLGA,PLGA-DC,RGD,LP-DC,LP-DC-RGD) in growth medium(GM). The old media from cells was aspirated and fresh 1ml of GM to cells was added. The diluted compounds prepared from new plate were transferred to old plate in the volume of 1ml into wells by starting from the lowest concentration. The plates were incubated for one, two and three population doubling time for both types of cells at 37°C in CO_2 incubator. The non-adherent and adherent cells were harvested in 5ml Falcon (352008) tubes. Cells were detached by using TrypLE solutions. Both types of cells were combined and pellet was made after centrifuging at 1500rpm/min. Cells were washed with ice cold PBS and stored overnight in 0.5ml of cold 70% ethanol (kept at -20°C). Cells were resuspended in 0.2ml of fresh made staining solution and data were acquired on FACScan and analysed by ModFit software. The composition of staining solution for 2000µl was water upto 2000 µl, propadium iodide (0.5mg/ml in water) 100 µl, triton X 100, (10%w/w) 10 µl and RNAse A 2.2 µl.

7.2.4. Apoptosis and Necrosis study

The cell suspension of 0.15 x 10^6 cells/ml was prepared for BT-20 cells in growth medium (GM) and was added 2.0 ml/well in 6 well plates. After 24hr, 2X sequential

dilutions of each compounds were prepared (DC,PLGA,PLGA-DC,RGD,LP-DC,LP-DC-RGD) in growth medium(GM). The old media from cells was aspirated and fresh 1ml of GM to cells was added. The diluted compounds prepared from new plate were transferred to old plate in the volume of 1ml into wells by starting from the lowest concentration. The plates were incubated for one, two and three population doubling time for both types of cells at 37°C in CO_2 incubator. The non-adherent and adherent cells were harvested in 5ml Falcon (352008) tubes. Cells were detached by using TrypLE solutions. Both types of cells were combined and pellet was made after centrifuging at 1500rpm/min. Cells were washed with ice cold PBS. The 1X binding buffer solution was made with 10mM HEPES, 140mM NaCl, and 2.5mM $CaCl_2$, pH7.4. The staining solution was prepared in 1X binding buffer with 4µl of Annexin V and 4µl of propadium iodide (100µg/ml) per each 100 µl of cell suspension. The control staining solution with single dye was prepared. 100 µl of staining solution was added to cell pellet. After 15 minutes incubation at room temperature, the 300µl of Annexin V binding buffer was added and samples were analyzed within one hour by flow cytometry. The data were analyzed by cell quest software.

7.2.5. Histological study by TEM

BT-20 Cells were seeded in 96 well plates with wells covered with sterile Acer plastic at the density of $1x10^5$ cells per well. After 24 hrs nanoconstructs dispersion in growth medium was prepared at the 2nM drug equivalent concentration and transferred to well containing cells. After 2 hrs, old medium was aspirated and cells were washed with PBS 7.4pH for three times. After washing cells were fixed in 4% buffered formalin and kept at 4^0C until analyzed by TEM.

7.3. Results and Discussion:

7.3.1. Intracellular uptake of Nanoparticles

Intracellular uptake of nanoparticles is often studied after incorporation of fluorescent dye in to the nanoparticles system. 6-coumarin has been widely used as a fluorescent marker to study the intracellular uptake of nanoparticles. The other advantages of 6-coumarin include the requirement of low dye loading in nanoparticles due to its high fluorescence activity (Panyam, J, et al., 2003). The uptake of these nanoparticles can be easily

visualized by fluorescence microscopy. Hence 6-coumarin loaded nanoparticles were used to study the intracellular uptake of the nanoparticles.

The factors affecting the particle cellular uptake primarily include particle size (Panyam, J. et al., 2003, Xie and Wang et al., 2005), different cell lines and cell densities (Jung et al., 2000), different compositions of the particles, surface properties (surface hydrophilicity and surface charge) (Sahoo, S. K. et al., 2002 & Foster et al., 2001). The dye does not leach from the NPs during the experimental time frame and therefore the fluorescence seen in the cells is caused by NPs and not by free dye.

We observed that the entrapment efficiency was 92.21 % (as discussed in chapter 5), suggesting incorporation of most of the dye added in to the nanoparticles. The particle size and zeta potential of 6-coumarin loaded unconjugated nanoconstructs and RGD-conjugated nanoconstructs was similar to that of drug loaded nanoconstructs hence, it is expected that their cellular uptake would be similar to drug loaded nanoconstructs.

Influence of concentration

The results of influence of the concentration on the intracellular uptake are shown in Table: 7.2 and graphically represented in Figure: 7.2.

Table: 7.2. Influence of concentration on the Cellular Uptake Efficiency

Concentration (µg/ml)	Cellular Uptake Efficiency			
	PLGA-DC	PLGA-DC-RGD	LP-DC	LP-DC-RGD
2	63.23± 3.27	84.36± 2.24	68.23± 3.48	85.28± 2.87
50	49.28 ± 3.21	81.18 ± 3.24	52.31 ± 1.82	84.12 ± 1.58
100	33.25 ± 3.73	63.81 ± 3.54	43.68 ± 2.39	78.34 ±3.21
200	26.28 ± 1.62	51.28 ± 1.81	35.26 ± 2.82	72.58 ± 3.75
500	19.83 ± 1.21	41.29 ± 1.42	26.47 ± 2.34	58.61 ±3.52

Figure: 7.2: Influence of Concentration on the Cellular Uptake Efficiency

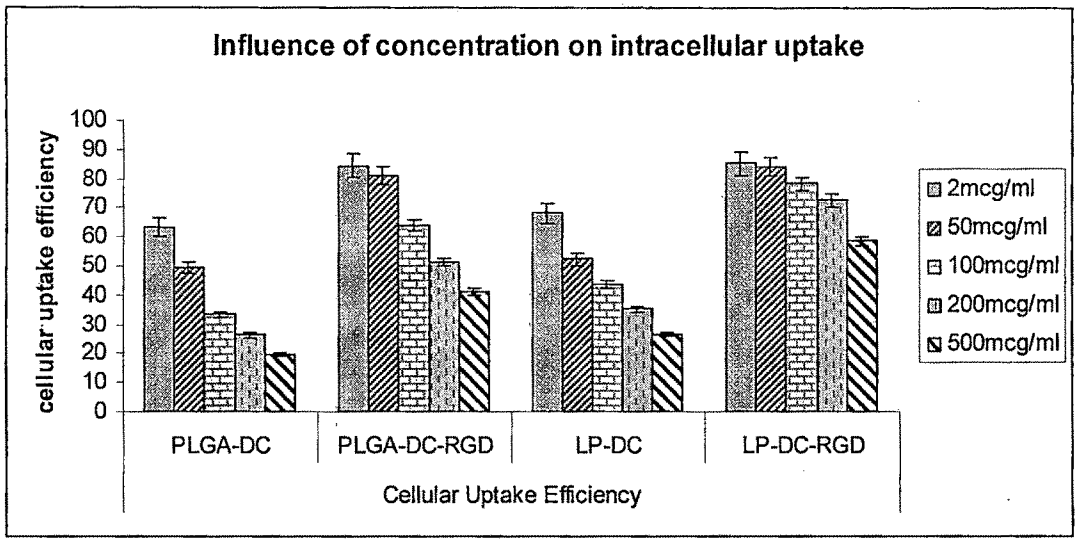

The uptake of the nanoparticles was directly proportional to the concentration of the nanoparticles in the medium. It was observed that the cellular uptake of the nanoparticles increased with increase in the concentration. However, the cellular uptake efficiency was found to be highest at the lowest concentration and found to decrease with increase in concentration. The decrease in the uptake efficiency indicates that the cells might have reached the saturating capacity for uptake. RGD-conjugated nanoconstructs at all concentrations demonstrate 1.6-2.1 folds increased uptake over unconjugated nanoconstructs uptake. The superior uptake of the RGD conjugated nanoparticles could be due to specific active endocytosis process mediated through the RGD adhesion to the integrins.

Influence of Incubation time

The quantitative uptake results of 6-coumarin loaded nanoconstructs are shown in Table: 7.3 representing the influence of the incubation time and graphically shown in Figure: 7.3.

Table: 7.3. Influence of Incubation time on the Cellular Uptake Efficiency

Time (hrs)	Cellular uptake efficiency			
	PLGA-DC	PLGA-DC-	LP-DC	LP-DC-RGD
0	0	0	0	0
0.25	7.31 ± 0.14	15.18 ± 0.12	10.21 ± 0.14	21.56 ± 1.21
0.5	13.54 ± 0.12	27.34 ± 0.38	17.33 ± 0.18	35.67 ± 1.32
1	20.23 ± 0.91	41.27 ± 1.26	25.46 ± 0.72	49.34 ± 2.76
2	29.23 ± 2.12	58.84 ± 1.32	35.67 ± 1.28	68.53 ± 1.48
4	38.45 ± 2.87	71.34 ± 2.18	44.45 ± 2.45	82.45 ± 3.12
5	40.58 ± 2.52	78.62 ± 2.41	48.34 ± 1.78	86.37 ± 2.84

Figure: 7.3. Influence of Incubation time on the Cellular Uptake Efficiency

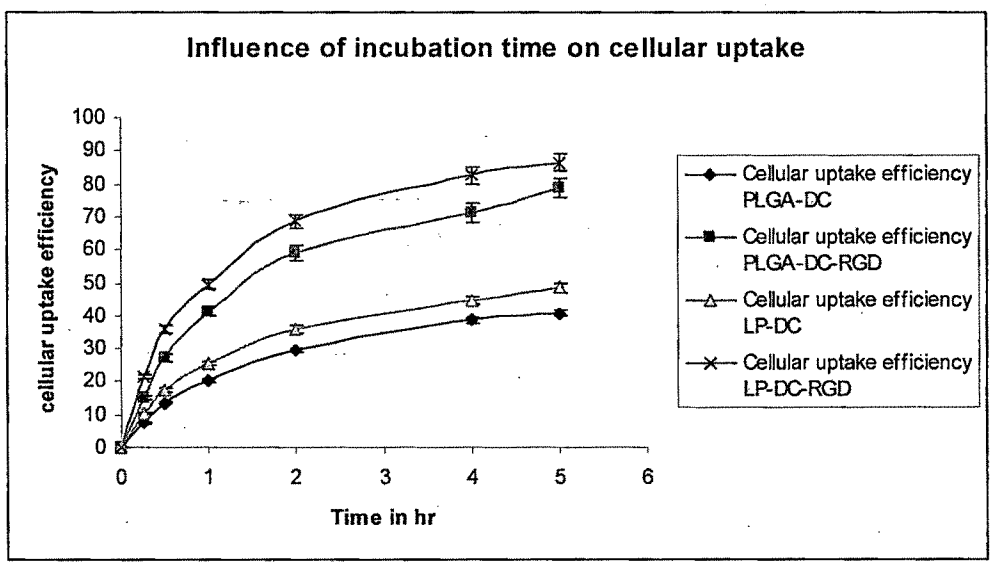

The results of quantitative uptake studies indicate the uptake of the nanoparticles into the cell. The untreated cells did not demonstrate any fluorescence. The nanoconstructs cell uptake efficiency was found to increase with time from 0.25-4hrs for both the unconjugated and RGD conjugated nanoconstructs. At all time points, the uptake efficiency of RGD conjugated systems were approximately 1.6~2.1 folds higher than the unconjugated systems. At 5hrs there was not much increase in the uptake efficiency suggesting the saturation of uptake with time. Hence, the influence of the concentration was performed by keeping the incubation time at 4hrs for all concentrations.

7.3.2. Fluorescent microscopy

The uptake of the nanoparticles in the cells was visualized by fluorescent microscopy (Figure: 7.4).

Figure: 7.4. Intracellular uptake of 6-coumarin loaded PLGA-NP and RGD-PLGA-NP formulations after different time points

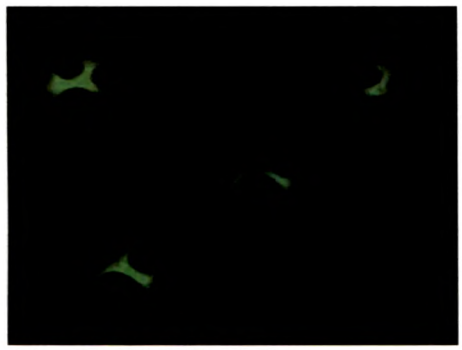

(a) PLGA-NPs-0.5hr

(b) RGD-PLGA-NPs-0.5hr

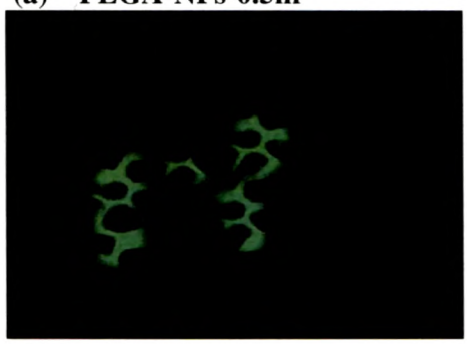

(c) PLGA-NPs-1hr

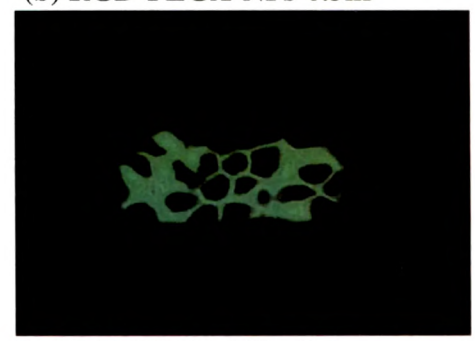

(d) RGD-PLGA-NPs-1hr

(e) PLGA-NPs-1.5hr

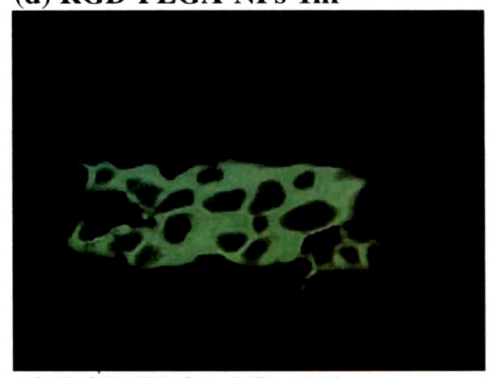

(f) RGD-PLGA-NPs-1.5hr

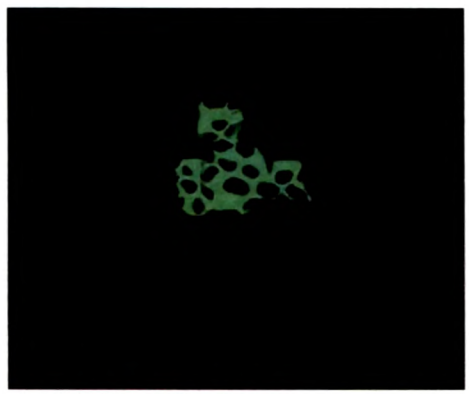

(g) PLGA-NPs-2hr

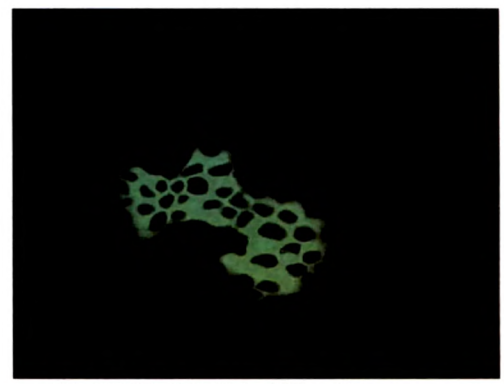

(h) RGD-PLGA-NPs-2hr

The fluorescent microscopic images showed green fluorescence in the cell cytoplasm and around the nucleus which reflects the internalization of the nanoparticles into the cell. Based on this observation, it is reasonable to believe that the nanoparticles may carry the active drug across the cell membrane into the cytoplasm. The RGD conjugated nanoparticles at all the time points demonstrated higher fluorescence intensity than the unconjugated nanoparticles confirming the results of the quantitative uptake studies. Also the RGD conjugated nanoparticles show higher number of the cells showing fluorescence than the unconjugated nanoparticles.

7.3.3. In-vitro Cytotoxicity Studies

The cell cytotoxicity is evaluated by assessment of viable cells after the treatment with drug or the formulation. Measurement of cell viability and proliferation forms the basis for numerous in vitro assays of a cell population's response to external factors. Cell Counting Kit-8 (CCK-8) allows very convenient assays by utilizing Dojindo's highly water-soluble tetrazolium salt. WST-8 [2-(2-methoxy-4-nitrophenyl)-3- (4-nitrophenyl)-5-(2,4-disulfophenyl)-2H-tetrazolium, monosodium salt] produces a water-soluble formazan dye upon reduction in the presence of an electron carrier.

Cell Counting Kit- 8, being nonradioactive, allows sensitive colorimetric assays for the determination of the number of viable cells in cell proliferation and cytotoxicity assays. WST-8 is reduced by dehydrogenases in cells to give a yellow colored product (formazan), which is soluble in the tissue culture medium. The amount of the formazan dye generated by the activity of dehydrogenases in cells is directly proportional to the number of living cells. The detection sensitivity of CCK-8 is higher than other tetrazolium salts such as MTT, XTT, MTS or WST-1.

To facilitate the basis of comparison the drug solutions, drug loaded nanoparticles & liposomes and drug loaded RGD conjugated nanoparticles & liposomes were added at same concentrations.

From the initial experiments, it was found that as compared to control (untreated cells), there was no significant cytoxicity observed for blank PLGA nanoparticles and blank liposomes and RGD itself at the highest concentration used in the study.

The cell viability results of Docetaxel and its nanoparticles formulations on BT-20 and MDA-MB-231 cells are given in Table: 7.4 & Table: 7.5 and graphically represented in

Figure: 7.5, and Figure: 7.6, respectively. The IC_{50} values observed for docetaxel and docetaxel nanoparticles are recorded in Table: 7.8 and Table: 7.9.

Similarly the cell viabilities for docetaxel and its liposomal formulations on BT-20 and MDA-MB-231 cells are given in Table: 7.6 & Table: 7.7 and graphically represented in Figure: 7.7 and Figure: 7.8. The IC_{50} values observed for docetaxel and docetaxel liposomes are recorded in Table: 7.10 and Table: 7.11.

Table: 7.4. Cell viability of Docetaxel and Docetaxel Nanoparticles on BT-20 cells

Conc. nM	Cell Viability (%) ± SD (n=3)								
	24hr			48hr			72hr		
	DC	PLGA-DC	PLGA-DC-RGD	DC	PLGA-DC	PLGA-DC-RGD	DC	PLGA-DC	PLGA-DC-RGD
50	45.6±2.3	44.4±1.8	41.4±1.05	24.9±1.2	15.8±1.3	10.8±0.82	5.2±0.56	2.8±0.14	1.8±0.22
25	51.7±4.1	52.8±2.9	49.3±2.1	35.8±2.5	29.4±1.7	12.4±0.56	7.4±0.63	6.4±0.34	3.6±0.45
12.5	71.6±3.5	70.4±1.6	68.4±2.7	52.5±2.6	42.8±2.1	18.5±1.4	13.7±0.92	11.4±0.91	5.4±0.43
6.25	81.4±4.5	79.2±2.3	76.4±3.2	62.4±3.1	59.4±2.6	29.6±1.3	21.6±1.6	15.4±0.98	11.5±0.93
3.125	91.3±4.8	85.4±3.8	83.2±4.2	72.6±3.7	69.8±3.2	41.8±2.1	44.1±2.6	29.8±1.6	19.7±1.2
1.5625	95.2±3.6	92.8±3.6	89.2±3.9	81.6±4.3	79.4±2.4	54.3±2.5	71.3±2.5	39.6±2.1	26.8±1.6
0.78125	96.3±2.9	94.3±2.8	92.5±4.1	89.4±4.7	85.4±4.1	65.6±3.1	83.4±4.1	48.4±2.1	39.4±2.1
0.390625	98.4±5.1	96.5±4.6	94.4±4.9	95.2±3.9	91.2±4.2	79.4±3.6	90.2±3.8	85.4±4.1	51.8±3.9
0.195313	99.4±4.7	98.4±4.2	96.2±5.2	98.2±5.3	94.2±3.8	89.4±4.3	94.6±5.3	90.2±4.2	88.7±4.1
0	104.2±3.8	103.4±5.2	104.8±5.5	106.4±5.2	105.4±5.4	102.8±4.2	106.8±5.1	102.7±3.8	103.2±4.5

(Mean±S.D., n=3)

Table: 7.5. Cell viability of Docetaxel and Docetaxel Nanoparticles on MDA-MB-231 cells

Conc. nM	Cell Viability (%) ± SD (n=3)								
	24hr			48hr			72hr		
	DC	PLGA-DC	PLGA-DC-RGD	DC	PLGA-DC	PLGA-DC-RGD	DC	PLGA-DC	PLGA-DC-RGD
50	41.3±0.98	39.5±2.7	21.4±1.7	19.5±0.78	11.6±0.32	10.5±0.21	1.2±0.05	1.5±0.03	1.4±0.05
25	49.6±1.4	45.4±1.1	41.4±1.8	25.4±0.45	19.4±1.2	15.4±0.43	2.4±0.11	2.1±0.02	1.8±0.04
12.5	59.2±1.5	56.8±1.2	52.8±1.5	39.8±0.79	33.8±2.1	23.8±0.35	4.8±0.31	3.5±0.05	2.5±0.03
6.25	64.2±1.9	61.7±3.2	58.7±2.1	52.7±1.6	42.4±1.7	32.7±1.1	9.4±0.25	5.7±0.12	4.9±0.45
3.125	75.4±2.3	72.3±2.4	69.3±1.3	69.6±1.7	51.2±1.5	41.4±2.1	19.8±0.98	11.8±0.23	10.4±0.67
1.5625	84.6±3.2	81.8±2.9	79.4±1.5	75.4±2.6	73.2±2.6	49.4±2.4	29.5±0.76	22.4±0.63	19.3±0.98
0.78125	91.5±2.9	87.4±3.2	85.6±2.3	83.4±2.8	80.1±3.8	71.6±3.1	52.2±2.1	41.4±1.3	35.5±2.1
0.39063	95.4±2.7	91.4±4.2	89.4±2.6	91.8±3.2	89.4±3.6	88.4±4.1	71.6±3.4	53.8±2.5	41.4±1.5
0.19531	97.2±3.8	95.2±3.4	94.9±4.3	95.4±4.2	93.3±6.1	91.6±5.2	89.7±5.6	89.2±5.1	52.8±3.4
0.09766	99.3±3,6	99.4±4.3	98.2±3.4	98.5±4.7	97.8±4.5	96.4±7.1	96.4±6.1	95.2±6.1	95.8±4.6
0	104.2±5.3	103.6±5.2	104.8±5.3	102.8±5.1	106.9±6.2	102.8±4.8	104.7±6.3	103.6±5.6.1	103.2±7.2

(Mean±S.D., n=3)

Table: 7.6. Cell viability of Docetaxel and Docetaxel Liposomes on BT-20 cells

Conc. nM	Cell Viability (%) ± SD (n=3)								
	24hr			48hr			72hr		
	DC	LP-DC	LP-DC-RGD	DC	LP-DC	LP-DC-RGD	DC	LP-DC	LP-DC-RGD
50	41.3±1.2	36.7±1.6	29.2±1.8	19.5±0.95	5.8±0.56	2.4±0.12	1.2±0.04	1.2±0.05	1.2±0.07
25	49.6±2.1	41.4±1.3	39.8±0.83	25.4±0.98	12.8±0.87	10.8±0.45	2.4±0.07	1.8±0.04	1.4±0.08
12.5	59.2±2.3	51.4±2.5	48.9±1.4	39.8±2.1	23.6±1.1	19.7±1.4	4.8±0.13	2.9±0.24	2.5±0.23
6.25	64.2±1.7	59.6±3.4	51.8±3.2	52.7±1.6	32.8±2.1	29.8±1.1	9.4±0.45	4.2±0.54	3.4±0.89
3.125	75.4±3.2	65.8±1.4	61.7±3.1	69.6±4.2	45.2±1.4	36.6±1.3	19.8±0.97	10.4±0.97	9.4±0.43
1.5625	84.6±2.8	72.6±2.8	68.6±4.9	75.4±5.6	65.2±3.2	46.8±1.2	29.5±1.1	19.8±1.1	15.8±0.85
0.78125	91.5±3.6	81.4±2.4	78.9±2.6	83.4±5.2	76.7±3.9	71.4±3.4	52.2±3.1	35.8±2.1	29.7±1.4
0.39063	95.4±2.3	85.4±4.9	81.4±4.1	91.8±4.3	85.8±4.7	84.6±2.7	71.6±4.2	45.8±3.1	39.4±3.2
0.19531	97.2±5.1	91.6±4.6	87.6±6.1	95.4±3.9	91.6±3.4	89.7±3.6	89.7±3.4	57.8±2.1	48.9±2.4
0.09766	99.3±5.3	97.4±3.7	95.7±4.9	98.5±5.8	95.4±5.1	94.9±4.6	96.4±5.1	75.7±4.5	74.6±3.3
0.04883	99.5±6.7	99.1±4.8	99.4±5.6	99.6±6.2	98.9±5.6	98.2±6.3	98.4±4.7	99.7±6.3	95.6±4.1
0	104.2±4.9	103.6±5.4	104.8±6.2	102.8±5.4	106.9±3.8	102.8±5.9	104.7±4.9	103.6±7.1	103.2±5.6

(Mean ± S.D., n=3)

Table: 7.7. Cell viability of Docetaxel and Docetaxel Liposomes on MDA-MB-231 cells

Conc. nM	Cell Viability (%) ± SD (n=3)								
	24hr			48hr			72hr		
	DC	LP-DC	LP-DC-RGD	DC	LP-DC	LP-DC-RGD	DC	LP-DC	LP-DC-RGD
25	51.7±2.3	41.4±1.2	35.4±2.3	35.8±1.3	13.7±0.76	5.8±0.45	7.4±0.56	1.5±0.04	1.5±0.04
12.5	71.6±3.6	49.2±3.2	48.1±2.5	52.5±1.4	25.9±1.4	11.2±0.75	13.7±0.87	2.9±0.06	3.1±0.06
6.25	81.4±2.8	68.5±3.4	66.5±1.3	62.4±3.2	39.4±1.2	17.6±0.56	21.6±0.99	9.4±0.32	5.9±0.11
3.125	91.3±3.1	75.4±4.1	73.8±4.2	72.6±2.5	52.8±2.3	27.2±2.3	36.4±1.4	13.8±0.15	10.5±0.24
1.5625	95.2±3.8	83.2±4.2	81.4±4.8	81.6±4.1	61.9±3.1	40.4±3.5	49.2±2.8	28.4±1.3	15.8±0.56
0.78125	96.3±5.3	89.4±4.8	88.6±3.5	89.4±3.4	71.8±2.3	53.9±2.8	83.4±3.9	37.8±3.2	24.7±1.3
0.39063	98.4±3.5	91.2±5.1	91.4±3.2	95.2±5.1	81.6±5.6	64.2±4.3	90.2±4.1	49.5±3.4	38.4±2.1
0.19531	99.4±4.2	95.4±4.3	93.2±5.1	98.2±3.2	89.4±4.3	78.6±3.5	94.6±4.9	84.6±5.1	49.6±2.5
0.09766	99.8±3.6	97.4±5.5	95.6±4.2	99.2±2.5	93.8±5.3	90.8±4.2	96.8±5.6	90.5±5.4	87.5±3.4
0	104.2±6.2	103.4±7.2	104.8±5.3	106.4±5.6	105.4±6.1	102.8±3.2	106.8±7.1	102.7±6.1	103.2±6.5

(Mean±S.D., n=3)

Figure: 7.5. Cell viability of Docetaxel and Docetaxel Nanoparticles on BT-20 cells at a) 24hrs, b) 48hrs and c) 72hrs

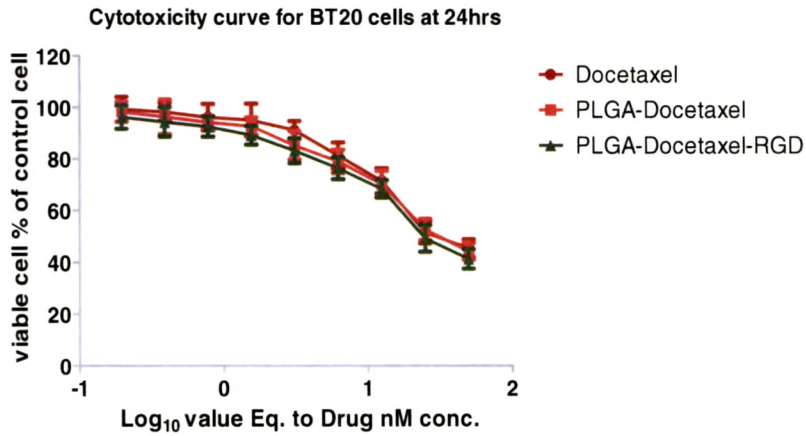

(a)

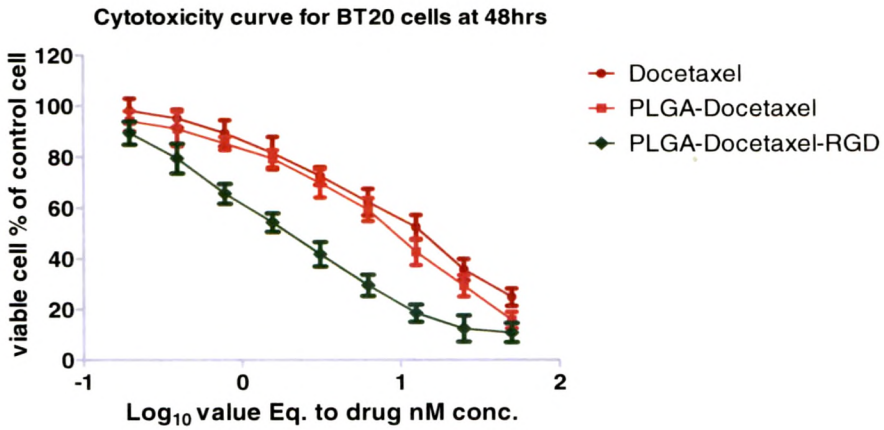

(b)

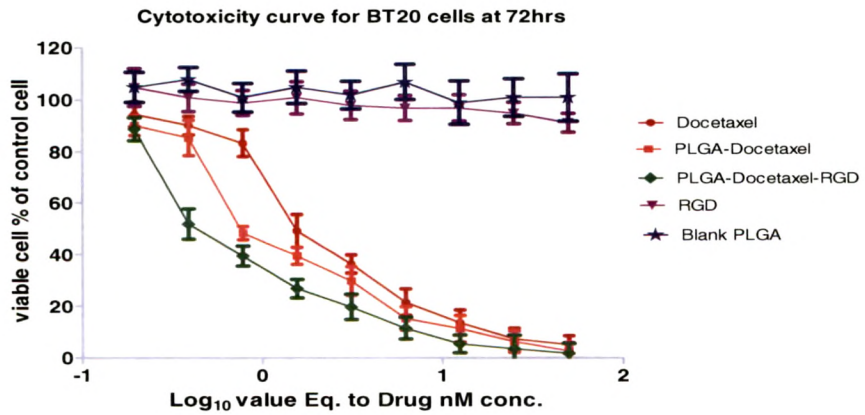

(c)

Figure: 7.6. Cell viability of Docetaxel and Docetaxel Nanoparticles on MDA-MB-232 cells at a) 24hrs, b) 48hrs and c) 72hrs

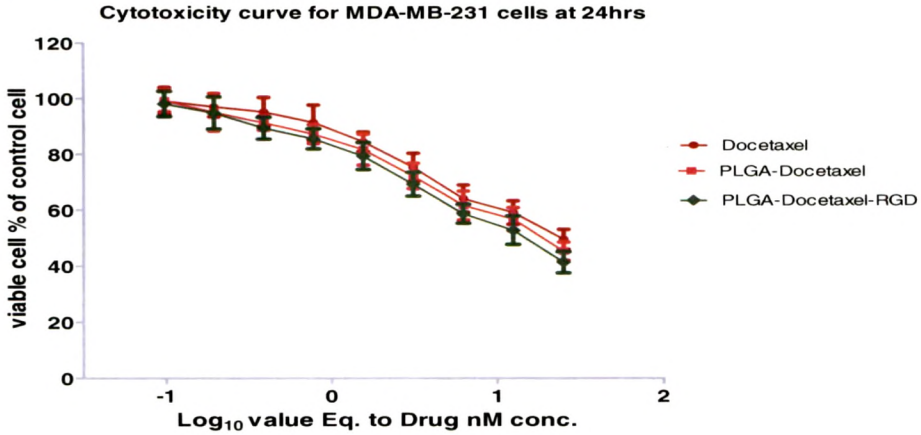

(a)

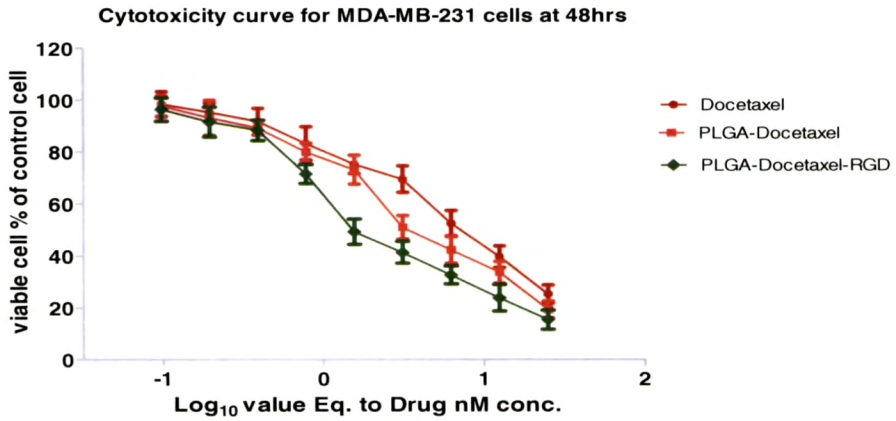

(b)

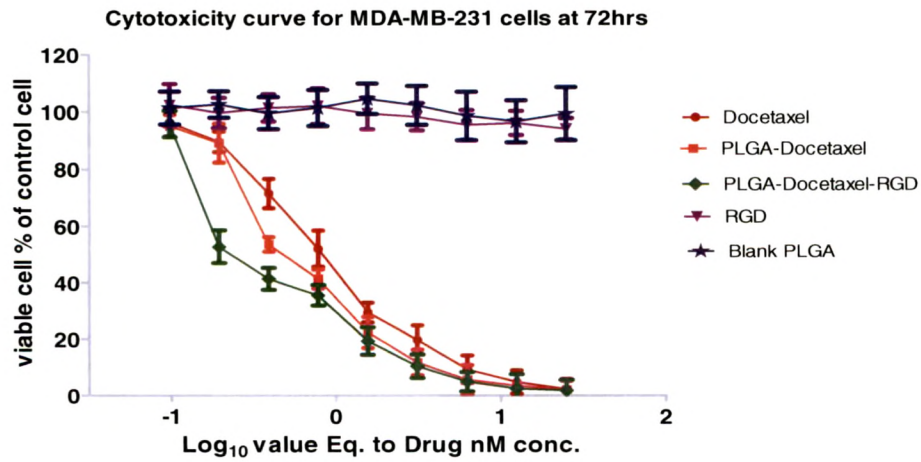

(c)

Figure: 7.7. Cell viability of Docetaxel and Docetaxel Liposomes on BT-20 cells at a) 24hrs, b) 48hrs and c) 72hrs

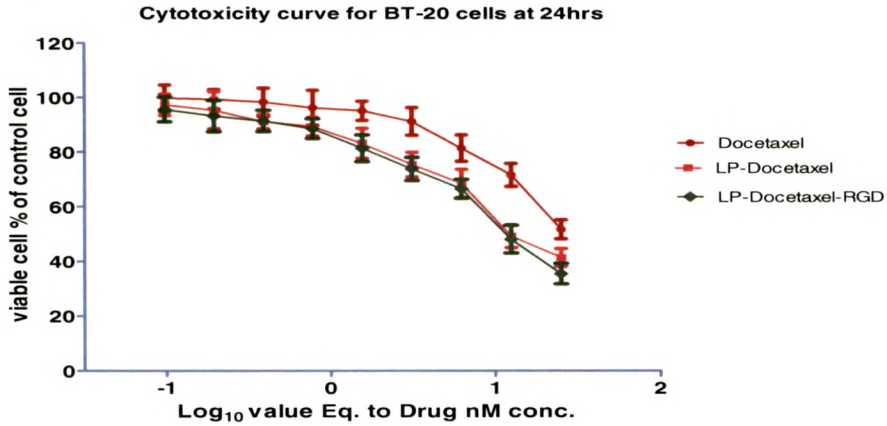

(a)

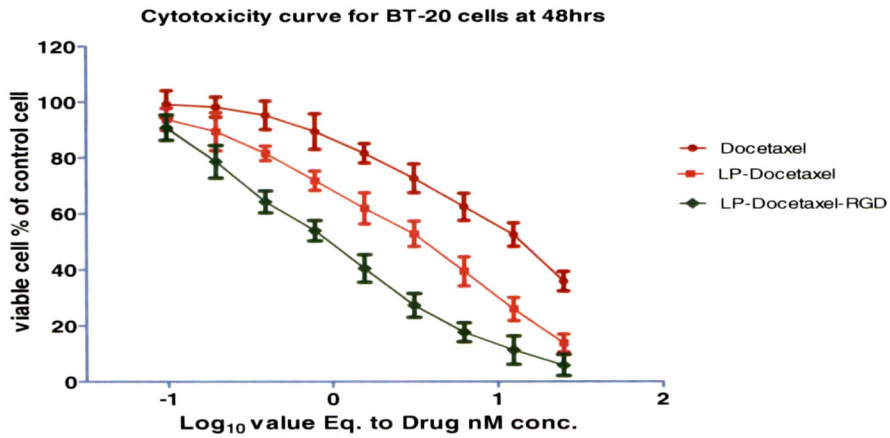

(b)

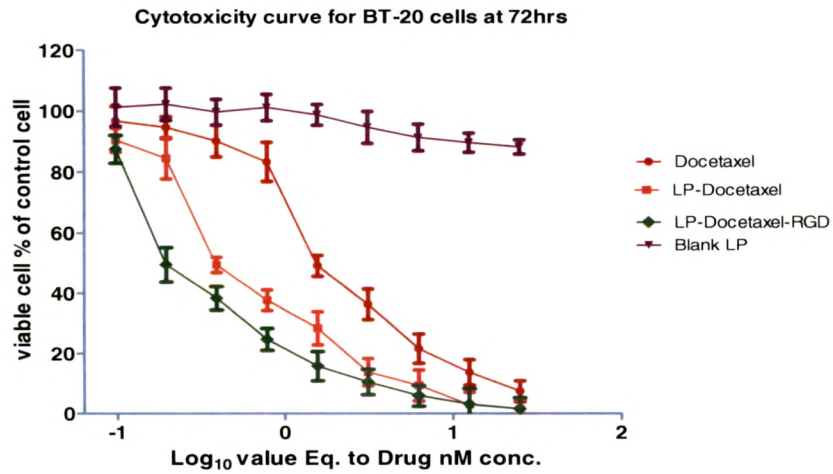

(c)

Figure: 7.8. Cell viability of Docetaxel and Docetaxel Liposomes on MDA-MB-231 cells at a) 24hrs , b) 48hrs and c) 72hrs

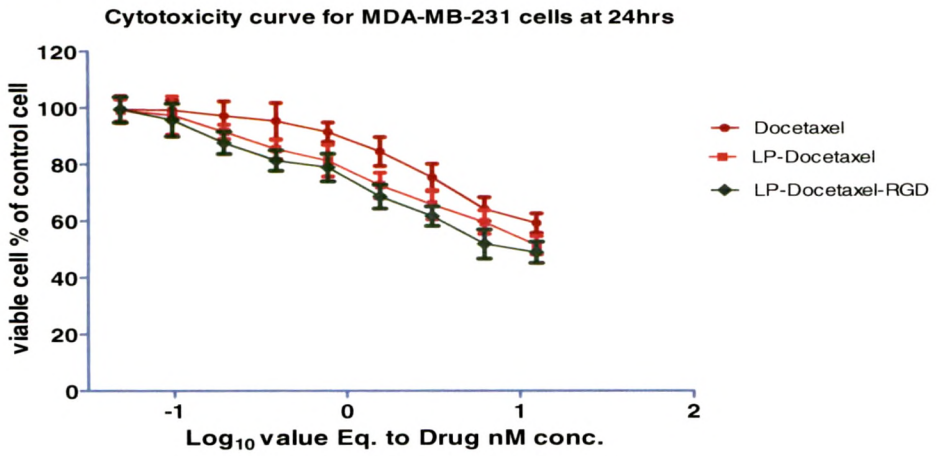

(a)

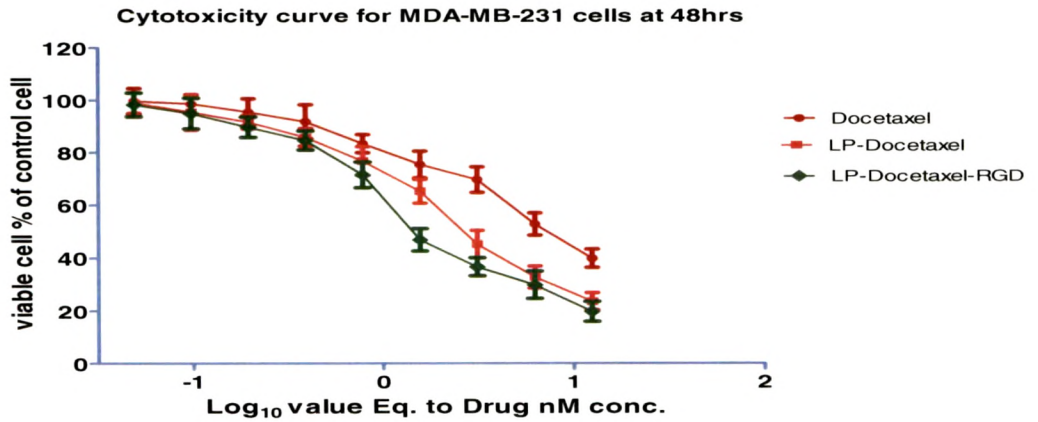

(b)

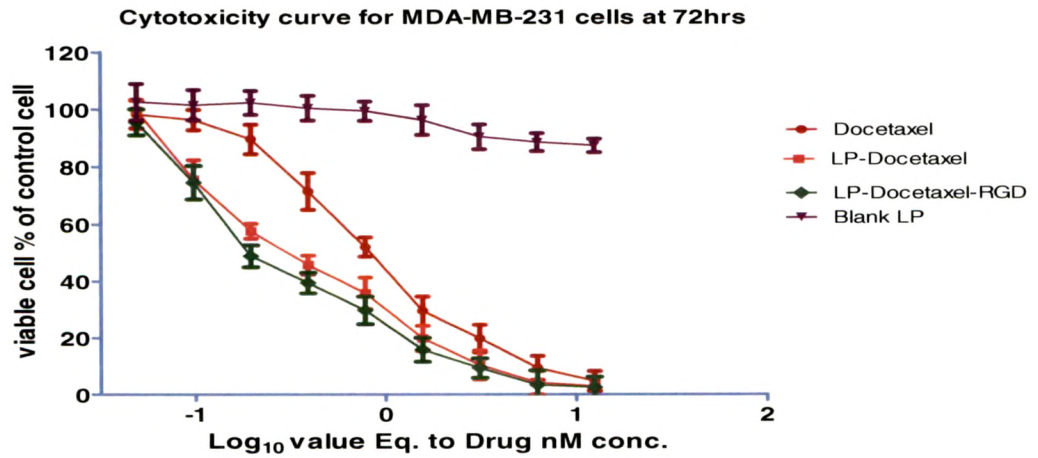

(c)

Table: 7.8. IC50 values for Docetaxel and Docetaxel Nanoparticles for BT-20 cell

Time (hr)	IC_{50} (nM)		
	DC	PLGA-DC	PLGA-DC-RGD
24	24.8±1.1	19.5±0.67	14.6±0.23
48	7.3±0.73	3.2±0.21	1.4±0.03
72	2.62±0.02	0.41±0.01	0.21±0.01

Table: 7.9. IC50 values for Docetaxel and Docetaxel Nanoparticles for MDA-MB-231 cells

Time (hr)	IC_{50} (nM)		
	DC	PLGA-DC	PLGA-DC-RGD
24	26.2±1.2	27.5±0.98	23.4±0.99
48	11.6±1.1	9.35±0.32	2.2±0.07
72	1.5±0.12	0.72±0.01	0.4±0.01

Table: 7.10. IC50 values for Docetaxel and Docetaxel Liposomes for MDA-MB 231 cells

Time (hr)	IC_{50} (nM)		
	DC	LP-DC	LP-DC-RGD
24	24.8±1.1	14.6±0.56	8.3±0,23
48	5.8±0.12	2.7±0.12	1.3±0.02
72	0.81±0.03	0.31±0.01	0.17±0.01

Table: 7.11. IC50 values for Docetaxel and Docetaxel Liposomes for BT-20 cells

Time (hr)	IC_{50} (nM)		
	DC	LP-DC	LP-DC-RGD
24	24.8±1.1	12.3±0.78	12.2±0.98
48	5.8±0.23	3.6±0.06	0.81±0.02
72	1.5±0.03	0.38±0.01	0.18±0.01

The cytoxicity of the drug loaded PLGA nanoparticles, RGD conjugated PLGA nanoparticles, liposomes and RGD conjugated liposomes formulations were significantly higher ($p<0.05$) than the docetaxel solution itself for both cell lines. The cytotoxicity was found to be dose dependent. The results demonstrate that the cell viability decreases with increase in drug concentration, indicating increase in the cytotoxicity of the drug and the Nanoconstructs. It was also observed that the cytotoxicity increased with incubation time. The cytotoxicity at all the time points i.e 24, 48 and 72 hrs was found to be in descending order as RGD conjugated drug loaded nanoconstructs > drug loaded nanoconstructs > drug solution.

For PLGA nanoparticles as shown in Table: 7.4 & Table: 7.5, at 24 hrs though the conjugated nanoparticles (PLGA-DC-RGD) showed higher toxicities than drug solution and unconjugated nanoparticles (PLGA-DC), the difference was insignificant ($p>0.05$). The drug solution was found to be more cytotoxic than the unconjugated nanoparticles (PLGA-DC) but the difference was insignificant ($p>0.05$). Any significant difference was not observed in cytotoxicity after 24hrs between any forms of drugs on BT-20 cell lines. However in case of MDA-MB-231 cells, the PLGA-DC-RGD showed significantly ($p<0.05$) higher toxicity than the unconjugated nanoparticles and drug solution. With increase in the incubation time, the toxicities of the drug and the nanoparticles were found to increase.

At 48 hrs, docetaxel solution produced significantly low toxicity than both unconjugated and RGD conjugated nanoparticles. Among the nanoparticles, the RGD conjugated nanoparticles showed significantly higher toxicity than unconjugated nanoparticles for both types of cell line.

At 72hrs, i.e. after three population doubling time, the RGD conjugated nanoparticles at dose of 1.5nM showed greater toxicities with about ~74% & ~80% cytotoxicity (26% & 20% viability) compared to ~60% & 78% and ~50% & ~73% cytotoxicity for unconjugated nanoparticles and drug solution for BT20 and MDA-MB-231 cell lines respectively. At higher concentrations there was not much difference between the cytotoxicites of drug solution and the nanoparticles formulations (at 72hrs).

The IC_{50} values of the solution and nanoparticles formulations as shown in Table: 7.8 & Table: 7.9, indicating decrease in IC_{50} values with increase in incubation time. The cytotoxicity indicated by IC_{50} values suggests that RGD conjugated nanoparticles at 72hrs are 2.1 and 4 time more cytotoxic than unconjugated nanoparticles and drug solution for BT-20 cell lines. Similarly, for MDA-MB-231 cells, the RGD conjugated nanoparticles are 2 and 10 time more cytotoxic than unconjugated nanoparticles and drug solution.

For liposomes, as shown in Table: 7.6 & Table: 7.7 at 24hrs the unconjugated liposomes (LP-DC) and RGD conjugated liposomes (LP-DC-RGD) showed a significant ($p<0.05$) high toxicity with compared to drug solution for both types of cells. While the RGD conjugated liposomes (LP-DC-RGD) showed a significant high toxicity with compared to untargeted liposomes for MDA-MB-231 cells but in case of BT-20, this difference is insignificant. The DC loaded liposomes and RGD conjugated DC liposomes expressed significant cytotoxic effect ($p<0.05$) at all other time points compared to the drug solution and unconjugated nanoparticles for both types of cell lines. As observed for PLGA nanoparticles, the cytotoxicity for drug loaded unconjugated and RGD conjugated liposomes also increased with increase in the dose and the incubation time. The RGD conjugated and unconjugated liposomes of DC depicted high cytoxicity than the free drug solution at high dose of 25nM for both types of cell lines.

The IC_{50} values are shown in Table: 7.10 & Table: 7.11 for docetaxel encapsulated liposomes. The cytotoxicity indicated by IC_{50} values suggests that RGD conjugated liposomes at 72hrs are 1.875 and 8.3 time more cytotoxic than unconjugated liposomes and drug solution for BT-20 cell lines. Similarly, for MDA-MB-231 cells, the RGD conjugated liposomes are 1.82 and 4.7 time more cytotoxic than unconjugated liposomes and drug solution.

Docetaxel being a substrate to P-gp could have been exocytosed and thereby reduced intracellular levels and hence lower cytotoxicities. The higher cytotoxicity with the nanoconstructs formulation for docetaxel may be attributed to the enhanced intracellular levels of drug available after internalization of the nanoparticles. The

nanoparticles after intracellular uptake act as drug reservoir and release the drug with sustained action.

The superior antiproliferative/cytotoxic effect action with RGD conjugated nanoparticles could be because of greater intracellular uptake of RGD conjugated nanoparticles via $\alpha_v\beta_3$ integrins compared with unconjugated nanoparticles and drug solution. The BT-20 and MDA-MB-231 cells are reported to show over expression of the $\alpha_v\beta_3$ integrins. (MD. Anderson cancer unit). The over expression of the $\alpha_v\beta_3$ integrins leads to selective receptor mediated endocytosis of the RGD conjugated nanoparticles and thereby resulting greater intracellular delivery than the unconjugated nanoparticles and drug solution. Additionally, *in vitro* release study (as discussed in chapter 5) indicates that about 36.8% and about 19.4% docetaxel is released from unconjugated and RGD conjugated nanoparticles respectively in 3 days. For liposomes, the release was found to be 49.7% and 55.6% for unconjugated and RGD conjugated liposomes respectively, in 2 days. This indicates the release of drug is rapid with liposomal system with compared to PLGA nanoparticles. This might contribute to high toxicity of the drug encapsulated liposomes compared to drug containing nanoparticles.

It was found that nanoparticles and liposomes were more toxic for MDA-MB-231 cells compared to BT-20 cells. The one of the difference between both the cell lines is population doubling time (PDT). The BT-20 has 48 hrs of PDT while MDA-MB-231 has 24hrs of PDT. The cell repair mechanism are believed to be more active with cells having long PDT as each phase of cell cycle is longer than the usual. This might be one of the reasons that the toxicity of drug is also high with MDA-MB-231 as compared to BT-20 cells.

The greater availability of the RGD conjugated nanoparticles combined with the sustained release has led to the superior cytotoxicity. In one of the reports suggested by *Kim et al. 2006*, that the cytotoxicity of the anticancer drugs is more at repeated low metronomic doses than a high conventional dose. The sustained release from the nanoparticles could have acted as low metronomic doses and demonstrated higher cytotoxicity than the drug solution acting as conventional high dose.

7.3.4. Cell cycle study:

Cell cycle analysis was done to determine the growth phase in which the cells were accumulating due to inhibition of cell cycle progression. Docetaxel inhibits cell growth and proliferation primarily through its effect on the cell cycle and induction of apoptosis and necrosis (Khuri, F.R. et al., 2003). In our studies, the mechanism of inhibition of cell proliferation was found to be mediated through inhibition of cell-cycle progression with a relatively higher percentage of cells in the G_2 phase and lower percentage of cells in the S phase in the group that was treated with drug-loaded nanoconstructs and with the drug in solution (Table: 7.12 to Table: 7.16).

Table: 7.12. Cell cycle arrest study with Docetaxel

	24hrs			48hrs		
Component	**G1**	**S**	**G2**	**G1**	**S**	**G2**
Control A	62.7±2.5	21.5±1.5	15.8±0.76	57.2±1.4	25.5±1.2	17.2±0.87
DC 10nM	40.2±1.2	24.6±1.8	35.2±1.3	7.3±0.11	3.9±0.23	88.6±3.9
DC 30 nM	31.6±1.1	19.7±1.2	48.7±1.4	3.80±0.12	3.5±0.12	92.6±4.8
DC 50 nM	19.5±3.1	15.8±0.99	64.7±3.5	3.4±0.54	4.6±0.11	91.8±5.3

Table: 7.13. Cell cycle arrest study with Docetaxel Nanoparticles (PLGA-DC)

Components	24hr			48hrs		
	G1	**S**	**G2**	**G1**	**S**	**G2**
Control	57.2±2.3	20.5±0.78	13.2±0.77	57.2±2.3	20.5±0.23	13.2±0.56
5nM	44.4±1.3	25.3±2.1	30.3±0.99	25.6±1.1	8.9±0.11	65.5±2.8
10nM	33.8±1.1	21.6±0.76	44.6±2.3	2.6±0.07	1.2±0.02	96.2±5.4
20nM	21.6±1.3	16.8±0.87	61.6±3.1	2.4±0.03	1.3±0.03	96.3±6.4
Blank PLGA	-	-	-	56.3±3.8	21.325±1.1	22.31±1.1

Table: 7.14. Cell cycle arrest study with RGD conjugated Docetaxel nanoparticles (PLGA-DC-RGD)

Components	G1	S	G2
5nM 24hrs	31.5±1.2	16.8±0.98	51.7±2.4
10nM 24hrs	17.6±0.45	14.2±0.89	68.2±2.9
5nM 48hrs	10.4±0.12	15.5±0.88	74.1±3.6
10nM 48hrs	2.3±0.05	1.4±0.01	96.3±5.5
RGD	58.8±3.2	21.9±1.1	19.3±0.56

Table: 7.15 Cell cycle arrest study with Docetaxel Liposomes (LP-DC)

	24hrs			48hrs		
Components	G1	S	G2	G1	S	G2
Control	57.2±2.3	20.5±1.4	13.2±0.95	59.2±2.3	24.5±0.53	16.2±0.73
5nM	38.6±1.2	15.7±1.5	45.7±1.5	23.4±0.62	9.7±0.13	66.9±3.2
10nM	25.6±1.4	12.8±1.1	61.6±3.1	3.1±0.04	1.4±0.03	95.6±4.2
20nM	15.6±0.25	11.7±0.22	72.7±3.3	2.1±0.05	1.5±0.04	96.4±4.5
Blank LP	-	-	-	59.7±3.2	23.6±0.72	16.7±0.94

Table: 7.16. Cell cycle arrest study with RGD conjugated Docetaxel Liposomes (LP-DC-RGD)

Component	G1	S	G2
5nM 48hrs	8.6±0.56	15.8±0.34	75.6±4.3
10nM 48hrs	2.5±0.06	1.2±0.02	96.3±4.8
5nM 24hrs	30.4±1.3	14.2±0.04	55.4±1.3
10nM 24hrs	13.5±0.98	5.6±0.78	80.9±5.6

Figure: 7.9. Cell cycle arrest study after 24hrs with DC (a) and after 48hrs with DC (b)

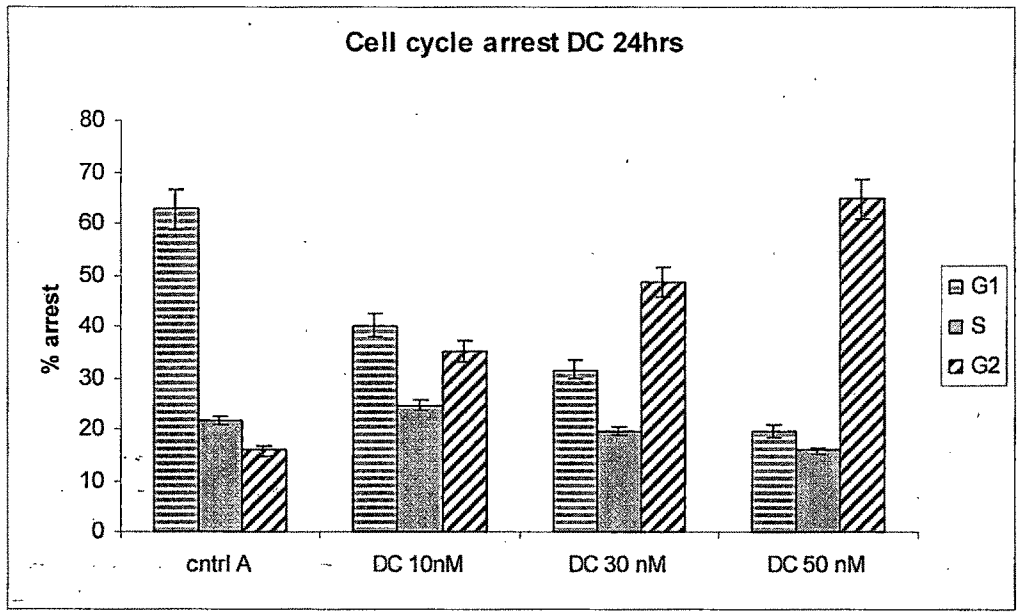

(a)

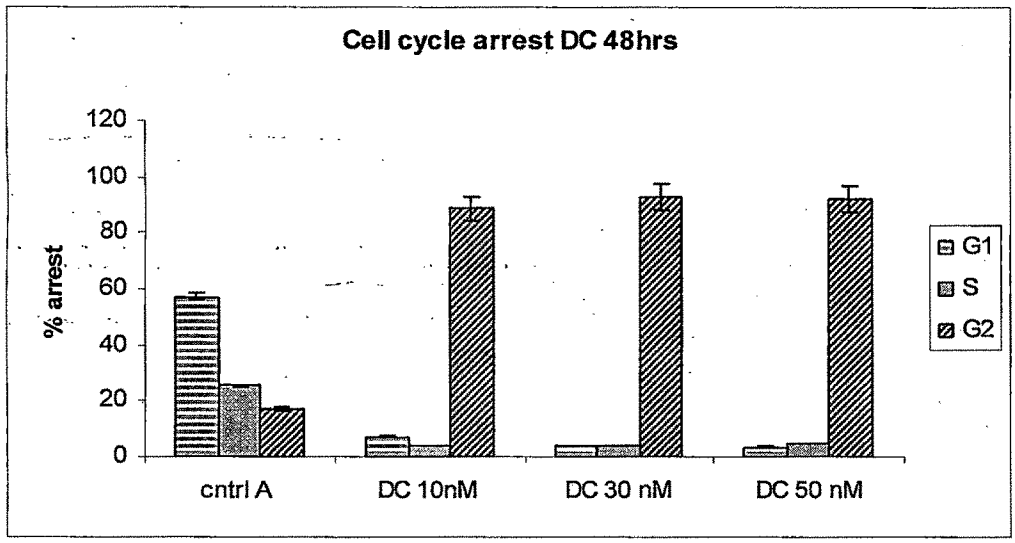

(b)

Figure: 7.10. Cell cycle arrest study after 24hrs with PLGA-DC (a), after 48hrs with PLGA-DC (b) and with PLGA-DC-RGD(c)

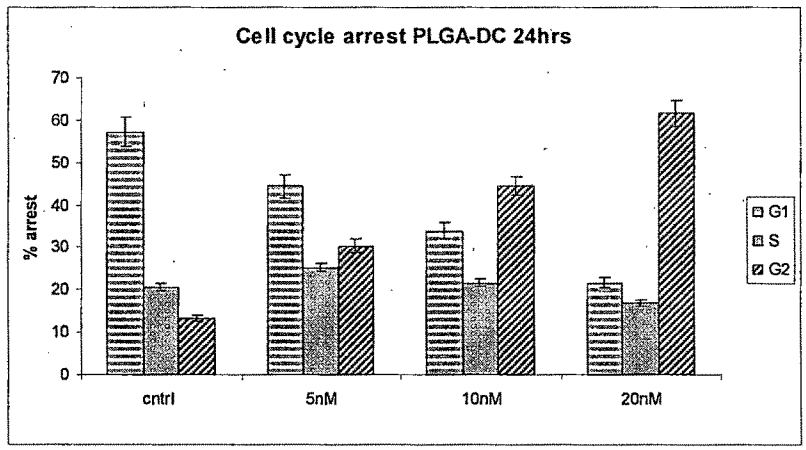

(a)

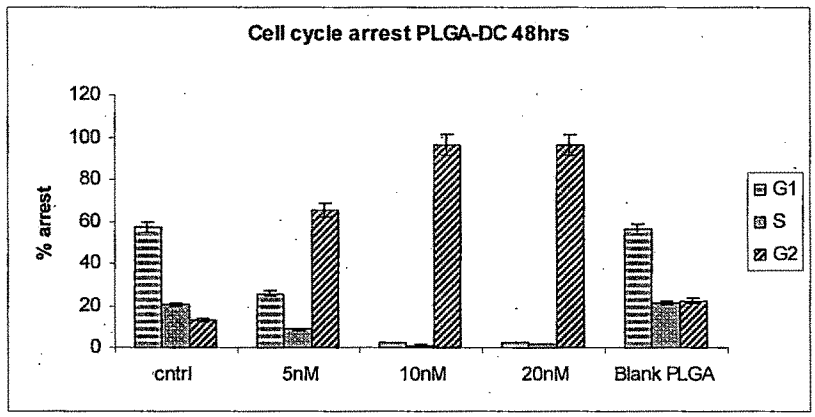

(b)

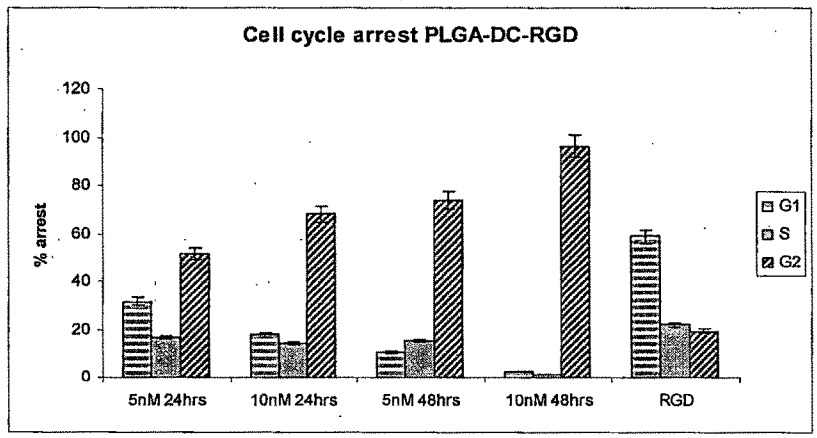

(c)

Figure: 7.11. Cell cycle arrest study after 24hrs with LP-DC (a), after 48hrs with LP-DC (b) and with LP-DC-RGD(c)

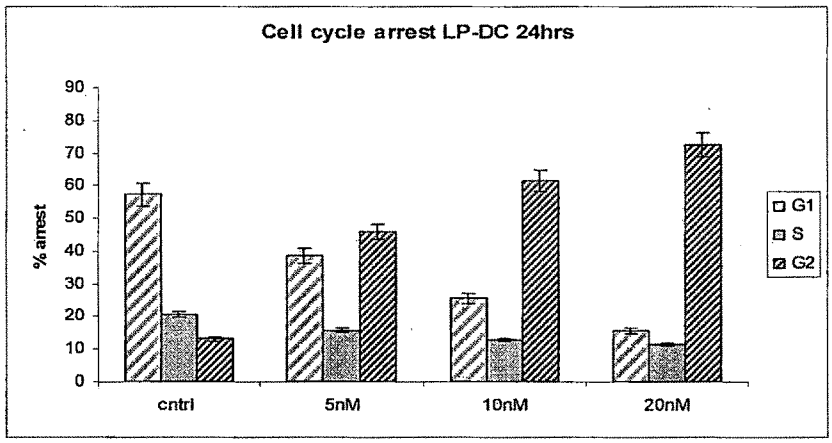

(a)

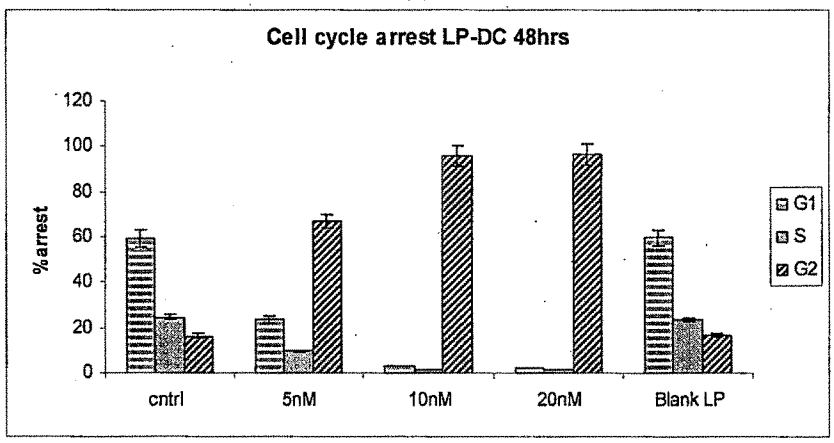

(b)

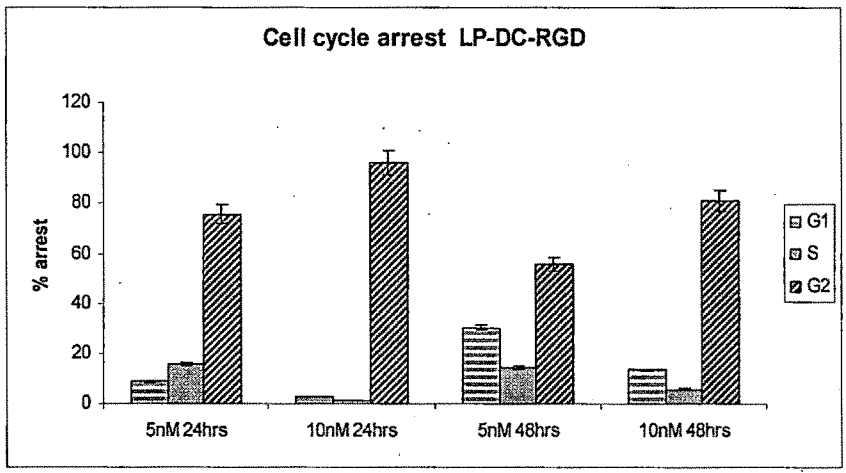

(c)

The study was done to find the effect of concentration and time. In case of free drug, the arrest in G2 phase was observed at lower concentration of 1nM and 2 nM but due to the high amount of debris, the exact percentage of each phase was difficult to calculate by Modfit software. At 24hrs, the cell cycle arrest in G2 phase was increasing significantly ($p<0.05$) as increase in concentration from 10nM to 30nM (Table: 7.12) for free drug. However, the difference was insignificant ($p>0.05$) at 48hrs between intra concentrations of free drug at 48hrs (Table: 7.12). It was observed at 48hrs, that with 10nM of free drug solution, the percentage G2 phase arrest was increased significantly compared to 24hrs effect. But the difference was insignificant with 30nM and 50nM of free drug. As shown in Table 7.14 the RGD conjugated nanoparticles at the drug equivalent concentration of 5nM showed 51% G2 phase arrest as compared to 30% G2 phase arrest with unconjugated nanoparticles at the same concentration at 24hrs (Table: 7.13). The block in G2 phase was found to be time and concentration dependent. At 48hrs, there is no significant difference between the effects of conjugated and unconjugated nanoparticles at 10nM concentration. Similarly, RGD conjugated drug encapsulated liposomal system was found to have significantly high arrest of cell cycle as compared to unconjugated system at same concentrations. The cell cycle arrest was found to be concentration and time dependent.

Cell cycle analysis demonstrated that all free DC, PLGA-DC and PLGA-DC-RGD arrested BT-20 cells in the G-2 phase of the cell cycle. However, in cells treated with PLGA-DC and PLGA-DC-RGD, the appearance of populations shown to be in G-2 was found to be more by at least 2 fold as compared to those treated with free DC. Further, the accumulation of cells in G-2 was accompanied by a 7–8 fold decrease in the number of cells in S phase compared to control cells, an indication of DNA replication inhibition. Blank PLGA and RGD peptide alone had no effect on cell cycle progression when applied using the same range of concentrations as PLGA-DC and PLGA-DC-RGD.

Figure: 7.12. DNA content analysis for BT-20 cells (a) control cell (b) Treated with IC50 eq. concentration of drug nanoparticles (c) Treated with 10nM drug eq. concentration of nanoparticles.

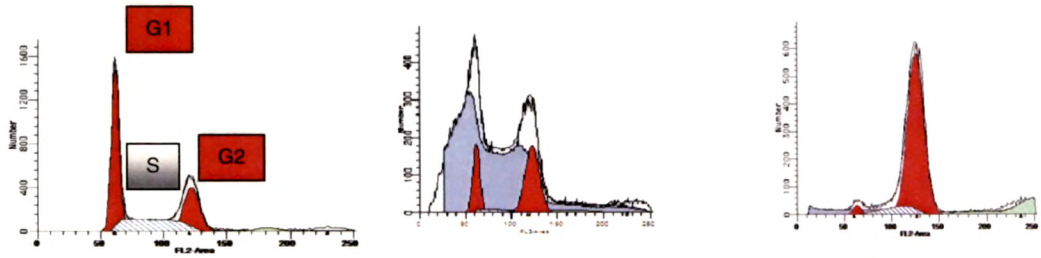

(a) (b) (c)

7.3.5. Apoptosis and Necrosis study:

The Apoptosis and Necrosis study was carried out to study the mode of cell death after the cell treatment with free drug solutions and drug containing nanoconstructs.

Figure: 7.13. Apoptosis and necrosis study with BT-20 cells (a) control cell (b) Treated with 0.5nM eq. concentration of drug nanoparticles (c) Treated with 0.25nM drug eq. concentration of nanoparticles.

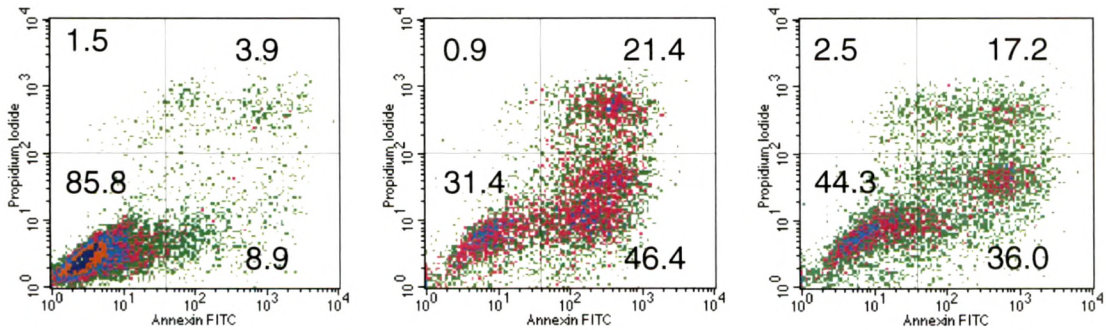

(a) (b) (c)

Table: 7.17. Apoptosis Necrosis study with Docetaxel, Docetaxel Nanoparticles and RGD conjugated Docetaxel Nanoparticles

Concentration	Components	24hr			48hr			72hr		
		Alive	Necrotic	Apoptotic	Alive	Necrotic	Apoptotic	Alive	Necrotic	Apoptotic
5nM	DC	85.3±3.2	13.6±0.45	1.1±0.01	65.4±3.2	22.4±1.1	2.2±0.06	30.4±2.1	66.2±4.1	3.4±0.04
	PLGA-DC	69.3±3.1	5.1±0.22	25.6±0.89	52.3±2.1	6.4±0.44	43.3±1.8	21.5±1.4	7.3±0.05	69.2±2.1
	PLGA-DC-RGD	65.3±1.2	6.4±0.11	28.3±1.1	35.2±0.69	5.6±0.35	59.2±1.1	15.4±1.1	3.3±p.06	81.3±3.4
10nM	DC	55.5±2.1	10.2±0.88	34.3±2.1	25.4±0.99	10.3±0.55	64.3±2.2	14.4±0.99	10.3±0.34	75.3±3.9
	PLGA-DC	44.2±1.1	8.4±0.56	47.4±2.3	15.3±0.57	10.3±0.23	74.4±3.4	10.3±0.33	11.3±0.25	78.4±5.1
	PLGA-DC-RGD	42.1±2.5	10.7±0.77	48.3±1.1	9.6±1.4	10.2±0.33	81.2±5.6	6.4±0.22	8.2±0.31	85.4±4.2

Table: 7.18. Apoptosis Necrosis study with Docetaxel, Docetaxel Liposomes and RGD conjugated Docetaxel Liposomes

Concentration		24hr			48hr			72hr		
	Components	Alive	Necrotic	Apoptotic	Alive	Necrotic	Apoptotic	Alive	Necrotic	Apoptotic
5nM	DC	85.3±4.5	13.6±0.05	1.1±0.02	65.4±3.2	22.4±1.2	2.2±0.02	30.4±1.2	66.2±3.2	3.4±0.03
	LP-DC	68.2±1.2	5.2±0.08	24.3±0.87	45.6±1.4	3.2±0.01	41.2±1.4	15.2±0.99	2.4±0.01	82.4±4.1
	LP-DC-RGD	64.3±1.6	6.5±0.23	29.7±0.98	20.8±1.1	2.1±0.03	77.1±2.2	7.3±0.55	3.3±0.03	89.4±3.4
10nM	DC	55.5±1.9	10.2±0.33	34.3±0.89	25.4±0.99	10.3±0.22	64.3±3.1	14.4±0.67	10.3±0.13	75.3±4.1
	LP-DC	38.4±2.1	11.4±0.55	50.2±1.6	15.5±0.79	9.3±0.31	75.2±3.7	7.2±0.15	7.4±0.23	85.4±3.8
	LP-DC-RGD	35.3±1.2	12.5±0.56	52.2±3.8	7.2±0.23	8.4±0.21	84.4±4.3	5.4±0.11	4.2±0.08	91.4±5.3

Figure: 7.14. Apoptosis Necrosis study with (a) Docetaxel, (b) Docetaxel Nanoparticles and (c) RGD conjugated Docetaxel Nanoparticles

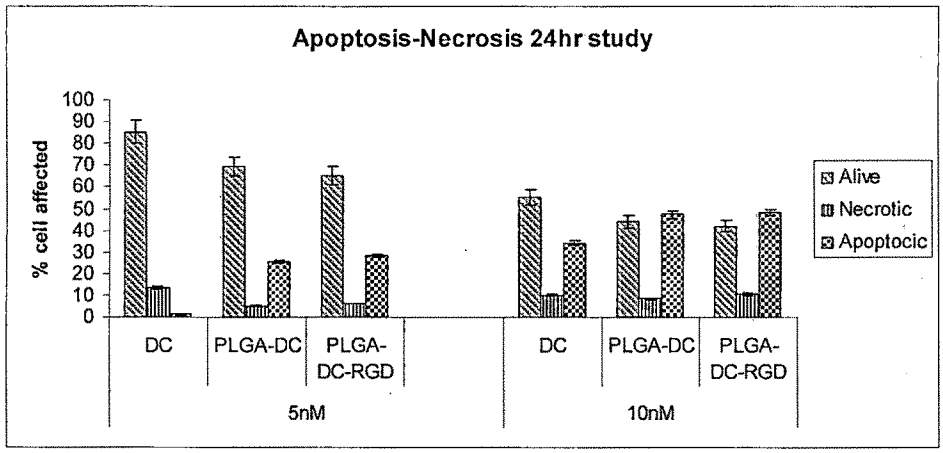

(a)

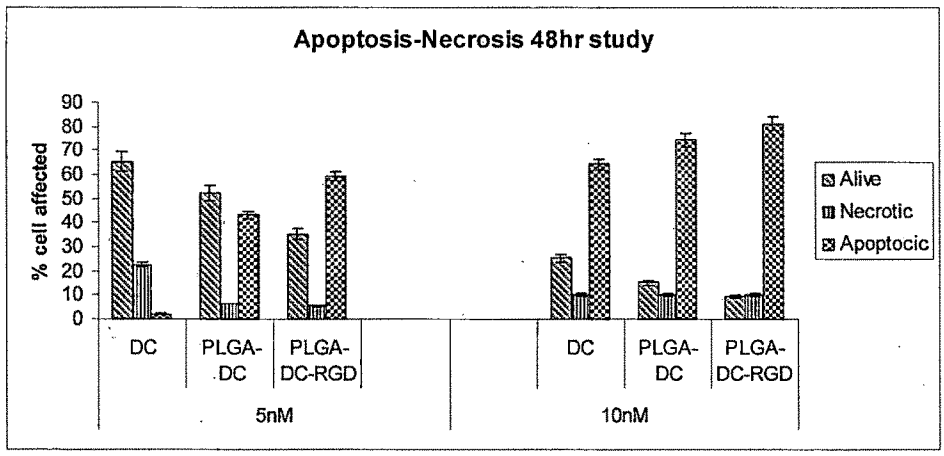

(b)

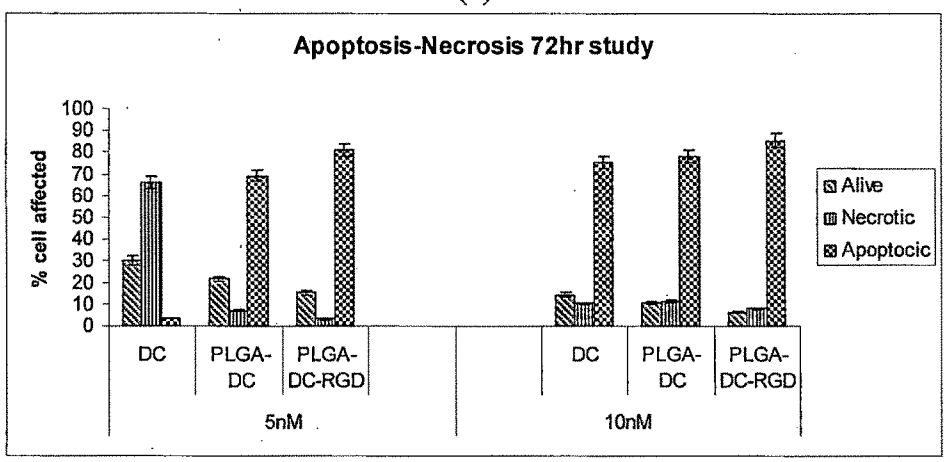

(c)

Figure: 7.15. Apoptosis Necrosis study with (a) Docetaxel, (b) Docetaxel Liposomes and (c) RGD conjugated Docetaxel Liposomes

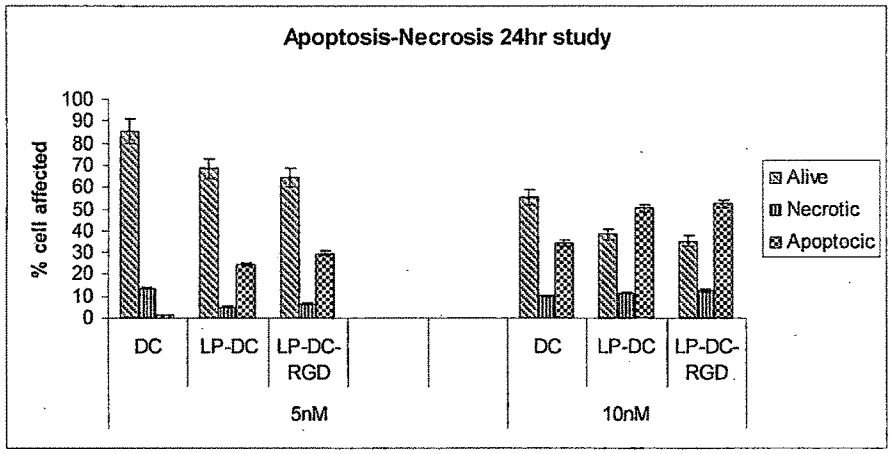

(a)

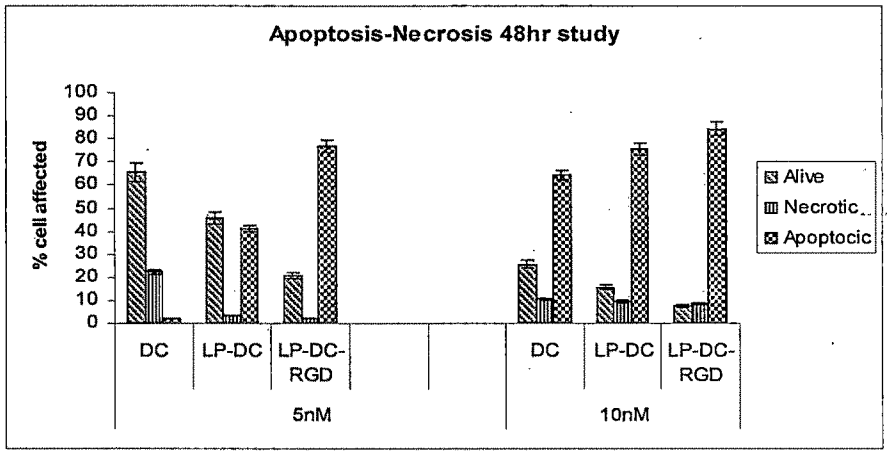

(b)

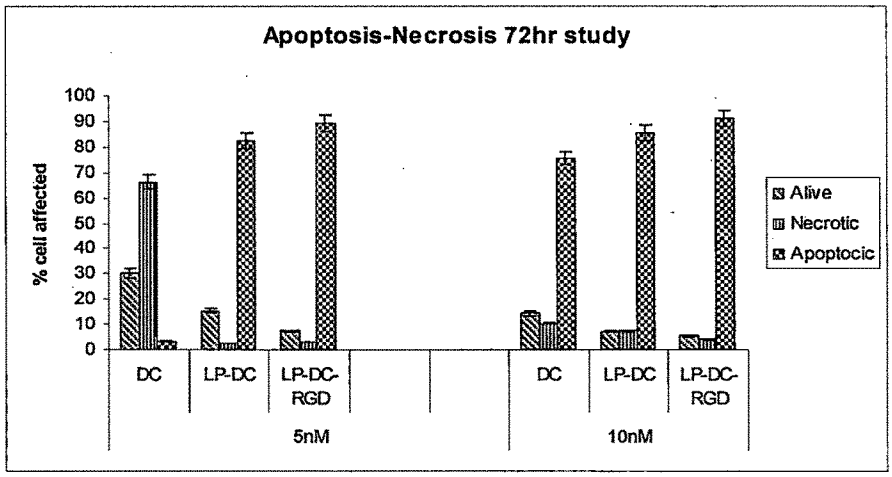

(c)

The apoptosis and necrosis effect was found to be concentration and time dependent for both types of drug delivery systems. In case of nanoparticles, the RGD conjugated nanoparticles have more apoptotic cell fragments than the unconjugated nanoparticles and drug solution at the same drug equivalent concentrations. At 24 hrs, the treatment of 5nM of drug solution with cells resulted in 13.6% & 3.4 % necrotic & apoptotic cell fragments, respectively. While at similar drug equivalent concentration, the PLGA-DC-RGD and PLGA-DC nanoparticles showed 6.4% & 28.3% and 5.1% & 25.6% necrotic & apoptotic cell fragments respectively. At 72hrs, the percent apoptotic cell fragments were significantly high for targeted nanoparticles as compared to untargeted nanoparticles and drug solution at 5nM concentration (Table: 7.17). While at 72hrs, the 5nM drug solution had significant high necrotic cell fragments as compared to targeted and untargeted Nanoparticulate systems. The free drug has found to have two mode of action at two different concentrations. At 5nM concentration it produces significantly high necrosis and low apoptosis. While at 10nM concentration the observed effect was reversed i.e. high apoptosis and low necrosis. The necrosis effect was significantly low in case of targeted and untargeted nanoparticles at both concentrations. At 10nM drug eq. concentration, the PLGA-DC-RGD nanoparticles have shown to be significantly high percentage of apoptosis with compared to same concentration of drug solution at all time points i.e. 24hrs, 48hrs and 72hrs. However the difference is insignificant with compared to PLGA-DC nanoparticles. Similar kinds of effects were observed with liposomal systems also (Table: 7.18).

We have shown that differences in the concentration of docetaxel will influence its mechanism of action at the molecular level, including cell cycle and cell death. In contrast, lower concentrations of free drug (2–4 nM) induce a high amount of cell debris. According to *Vargas H.H et a, 2007*, who has studied the dependency of this effect on cell cycle phase and concluded that docetaxel at lower concentrations is able to induce aberrant mitosis and aneuploidy. Currently, there are no experimental data to explain these findings, although several lines of evidence can shed light onto this issue. Docetaxel is easily accumulated in cells and produces impairment of microtubules. This impairment produces a moderate stabilization of p53 protein, followed by an induction of p53

transactivation activity once mitotic arrest is overcome. In contrast, docetaxel accumulation after higher doses of the drug induces a sustained arrest in mitosis with the consequent inhibition of transcription and higher p53 accumulation. Owing to an unknown mechanism, this difference in mitotic arrest duration also affects the postmitotic consequences, that is, aberrant mitosis with production of hypodiploid cells (at 2–4 nM docetaxel) vs mitosis slippage without cytokinesis producing large multinucleated cells (at 10-100 nM docetaxel). Moreover, as a consequence of this, the type of cell death will also be different, that is, mainly non-apoptotic after asymmetrical division, and mainly apoptotic after multinucleation. According to *Blagosklonny, et al 2006* model, mitotic arrest will induce p53 accumulation owing to the lack of transcriptional regulation of p53 during mitosis. After slippage, cells recover transcriptional ability and p53 protein will induce transcriptional targets, including p21. In agreement with Blagosklonny hypothesis, our data point to a mechanism regulating the different consequences of Docetaxel exposure according to the duration of mitotic arrest, depending on the accumulation of proteins (including p53 family of transcription factors) in a moment of the cell cycle when there is no transcriptional activity. Timing of arrest would determine the amount, and probably also the quality or type, of protein/s that will accumulate.

The consequences of a better understanding of the mechanisms of action of docetaxel are important. Mitotic perturbations will determine the main mechanism of cell death after docetaxel exposure. Similar to our results, *Fabbri et al 2006* found that lower concentrations of docetaxel were not able to induce early apoptosis (Annexin V, PI cells) in a bladder cancer cell line, and instead it induced a necrotic type of cell death. In a similar way, the ability of paclitaxel to induce cell death by independent mechanisms has been studied in more detail than docetaxel. It has been described that paclitaxel-dependent cytotoxicity requires cells to be first arrested at mitosis and upon mitotic slippage to enter apoptotic cell death (Blajeski et al., 2001). Moreover, differences in mechanism of action according to drug concentration have also been described with paclitaxel. In the early work of *Torres K, et al 1998*, aberrant mitosis was induced by low concentrations of paclitaxel followed by nonapoptotic cell death, and high concentrations induced mitotic arrest with apoptosis. In addition, according to *Giannakakou et al 2001*,

low concentrations of paclitaxel (between 6 and 12 nM) induce p53, p21 and G1/G2 arrest in MCF7 cells, instead of mitotic arrest.

7.3.6. Histology study by TEM:

The results are shown in Figure: 7.16a, Figure: 7.16b and Figure: 7.16c for Control cell, LPs-DC-RGD and PLGA-DC-RGD-NPs, respectively. Photomicrograph by TEM depicted that the RGD conjugated drug encapsulated liposomes were able to enter the nucleus of the BT-20 cells. While nanoparticles were found to be present in cell cytoplasm of breast cancer cells.

Figure: 7.16. Histology studies by TEM (a) Control cell (b) LPs-DC-RGD (c) PLGA-DC-RGD-NPs

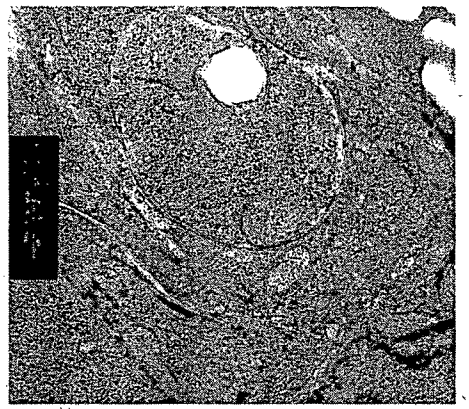

(a)

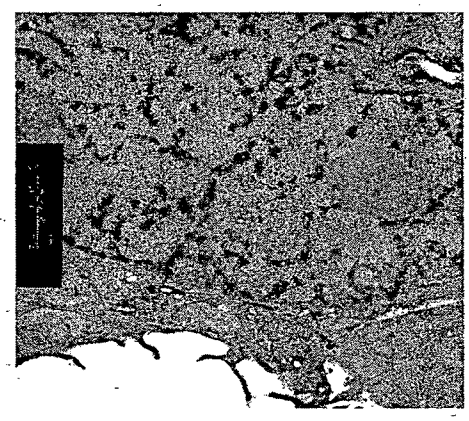

(b)

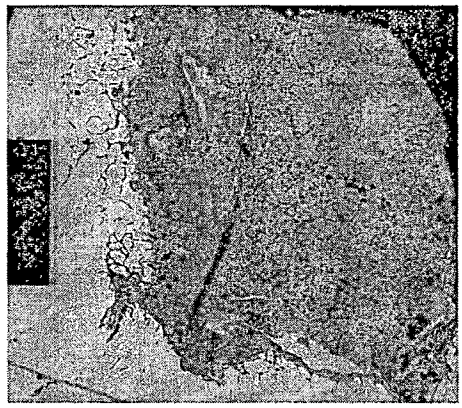

(c)

7.4. Conclusions

The blank PLGA nanoparticles and liposomes demonstrated no cytotoxicity on breast cancer cells suggesting the use of these nanoconstructs for safe delivery of anticancer agents. These nanoconstructs demonstrated higher cytotoxicity than drug solution due to high intracellular uptake of nanoconstructs and the prolonged release of drug from the nanoconstructs. RGD conjugated nanoconstructs due to receptor mediated uptake demonstrated significantly higher intracellular uptake and cytoxicity than unconjugated nanoconstructs and drug solution. The higher intracellular uptake of the RGD conjugated nanoparticles was confirmed by fluorescence microscopy. At the same drug equivalent concentrations, targeted docetaxel encapsulated nanoparticles and liposomes have shown high DNA content in G2 phase of cell cycle and more apoptotic cell fragments than untargeted systems and free drug solutions. Hence, it can be concluded that these nanoparticles and liposomes are suitable carriers to deliver docetaxel intracellularly for higher and prolonged cytotoxic effect.

7.5. References

Blagosklonny, M.V. et al., 1996, Taxol-induced apoptosis and phosphorylation of Bcl-2 protein involve c-Raf-1 and represent a novel c-Raf-1 signal transduction pathway, Cancer. Res., **56**, 1851–1854.

Blajeski, A.L. et al., 2001, A Multistep Model for Paclitaxel-Induced Apoptosis in Human Breast Cancer Cell Lines, Exp. Cell. Res., **270**, 277–288.

Foster K. A. et al., 2001, Microparticulate uptake mechanism of in-vitro cell culture models of the respiratory epithelium, J. Pharm. Pharmacol., **53**, 57-66.

Giannakakou, P. et al.,2001, Low concentrations of paclitaxel induce cell type-dependent p53, p21 and G1/G2 arrest instead of mitotic arrest: molecular determinants of paclitaxel-induced cytotoxicity, Oncogene, **20**, 3806–3813.

Jung T. et al., 2000, Biodegradable nanoparticles for oral delivery of peptides: is there a role for polymers to affect mucosal uptake, Eur. J. Pharm. Biopharm., **50**,147-160.

Khuri, F.R. et al., 2003, Mode of action of docetaxel – a basis for combination with novel anticancer agents, Cancer Treatment Reviews, **29**, 407–415.

Kim, et al., 2006, Metronomic treatment of temozolomide inhibits tumor cell growth through reduction of angiogenesis and augmentation of apoptosis in orthotopic models of gliomas, Oncology reports, **16**, 33-39.

Korsmeyer, S.J., et al., 1993, Sem. Cancer Biol., **4**, 327-332.

Panyam, J. et al., 2003, Fluorescence and electron microscopy probes for cellular and tissue uptake of poly(D,L-lactide-co-glycolide) nanoparticles, Int. J. Pharm., **262**, 1-11.

Reed, J.C. et al., 1994, J. Cell Biol., **124**, 1-6.

Sahoo, S. K. et al., 2002, Residual polyvinyl alcohol associated with poly (D,L-lactide-co-glycolide) nanoparticles affects their physical properties and cellular uptake, J. Control. Rel., **82**, 105-114.

Sahoo, S. K. et al., 2004, Efficacy of transferrin-conjugated paclitaxel-loaded nanoparticles in a murine model of prostate cancer, Int. J. Cancer, **112,** 335–340.

Sahoo, S. K. et al., 2005, Enhanced Antiproliferative Activity of Transferrin-Conjugated Paclitaxel-Loaded Nanoparticles Is Mediated via Sustained Intracellular Drug Retention, Molecular Pharmaceutics, **2 (5)**, 373-383.

Steller, H. et al., 1995, Science, **267**, 1445-1449.

Torres, K. et al., 1998, Mechanisms of Taxol-induced cell death are concentration dependent, Cancer Res., **58**, 3620–3626.

Vargas, H. H. et al., 2007, Molecular profiling of docetaxel cytotoxicity in breast cancer cells: uncoupling of aberrant mitosis and apoptosis, Oncogene, **26**, 2902–2913.

Wyllie, A.H. et al., 1980, Int. Rev. Cytol., **68**, 251-306.

Xie J. et al., 2005, Self-Assembled Biodegradable Nanoparticles Developed by Direct Dialysis for the Delivery of Paclitaxel, Pharmaceutical Research, **22(12)**, 2079-2090.

Zakeri, Z. et al., 1995, Death and Differentiation, **2**, 87-96.

Zhong, L.T. et al., 1993, Proc. Natl. Acad. Sci. USA, **90**, 4533-4537.

Zsolt Bacso et al., 2000, Cancer Research, **60**, 4623–4628.

Chapter 7 255
7.1. Introduction 256
7.2. Methods 260
7.2.1. Intracellular uptake studies 260
7.2.2. In-vitro Cytotoxicity Studies 261
7.2.3. DNA content anlaysis by flow cytometry 262
7.2.4. Apoptosis and Necrosis study 262
7.2.5. Histological study by TEM 263
7.3. Results and Discussion: 263
7.3.1. Intracellular uptake of Nanoparticles 263
7.3.2. Fluorescent microscopy 266
7.3.3. In-vitro Cytotoxicity Studies 268
7.3.4. Cell cycle study: 282
7.3.5. Apoptosis and Necrosis study: 288
7.3.6. Histology study by TEM: 294
7.4. Conclusions 295
7.5. References 296